

# General-relativistic hydrodynamics of non-perfect fluids: 3+1 conservative formulation and application to viscous black-hole accretion

Michail Chabanov<sup>1</sup>, Luciano Rezzolla<sup>1,2,3</sup> and Dirk H. Rischke<sup>1</sup>

<sup>1</sup>*Institut für Theoretische Physik, Goethe-Universität, Max-von-Laue-Str. 1, 60438 Frankfurt am Main, Germany*

<sup>2</sup>*Frankfurt Institute for Advanced Studies, Ruth-Moufang-Str. 1, 60438 Frankfurt am Main, Germany*

<sup>3</sup>*School of Mathematics, Trinity College, Dublin 2, Ireland*

Accepted XXX. Received YYY; in original form ZZZ

## ABSTRACT

We consider the relativistic hydrodynamics of non-perfect fluids with the goal of determining a formulation that is suited for numerical integration in special-relativistic and general-relativistic scenarios. To this end, we review the various formulations of relativistic second-order dissipative hydrodynamics proposed so far and present in detail a particular formulation that is fully general, causal, and can be cast into a 3+1 flux-conservative form as the one employed in modern numerical-relativity codes. As an example, we employ a variant of this formulation restricted to a relaxation-type equation for the bulk viscosity in the general-relativistic magnetohydrodynamics code BHAC. After adopting the formulation for a series of standard and non-standard tests in 1+1-dimensional special-relativistic hydrodynamics, we consider a novel general-relativistic scenario, namely, the stationary, spherically symmetric viscous accretion onto a black hole. The newly developed solution – which can exhibit even considerable deviations from the inviscid counterpart – can be used as a testbed for numerical codes simulating non-perfect fluids on curved backgrounds.

**Key words:** hydrodynamics, shock waves, accretion

## 1 INTRODUCTION

The detection of the first binary neutron-star (BNS) merger event, GW170817 ([Abbott et al. 2017a](#)) has provided a new valuable tool to study matter and gravity under extreme conditions. Especially the detection of electromagnetic counterparts in form of a short gamma-ray burst ([Abbott](#)

et al. 2017b) and of a kilonova (Drout et al. 2017; Cowperthwaite et al. 2017) accompanying GW170817, has made this event an incredibly rich laboratory for physics, providing a number of constraints on the equation of state (EOS) of nuclear matter (see, e.g., Margalit & Metzger 2017; Bauswein et al. 2017; Rezzolla et al. 2018; Ruiz et al. 2018; Annala et al. 2018; Radice et al. 2018b; Most et al. 2018; De et al. 2018; Abbott et al. 2018; Montaña et al. 2019; Raithel et al. 2018; Tews et al. 2018; Malik et al. 2018; Koepfel et al. 2019; Shibata et al. 2019).

BNS mergers are highly dynamical and nonlinear phenomena especially during the first few milliseconds after merger, (see, e.g., Baiotti & Rezzolla 2017; Paschalidis 2017; Burns 2020, for some reviews). As has been shown recently, harmonic density oscillations in this violent phase could be damped significantly due to bulk-viscosity dissipation coming from modified Urca processes (Alford et al. 2018, 2020; Alford & Haber 2020). Thus, bulk viscosity might lead to modifications in the post-merger gravitational-wave signal. Furthermore, it was shown in high-resolution general-relativistic magnetohydrodynamic (GRMHD) calculations that the matter after merger is unstable to MHD instabilities, e.g., the Kelvin-Helmholtz instability (Baiotti et al. 2008; Radice & Rezzolla 2012) and the magnetorotational instability (Siegel et al. 2013; Kiuchi et al. 2018). Due to these instabilities, turbulence can develop and be maintained, which will ultimately influence BNS-merger observables such as the gravitational-wave signal and the ejected matter.

The emergence of turbulence clearly represents a challenge for numerical-relativity simulations, which can only be performed with limited resolutions and are normally carried out with resolutions that are well above the scale at which turbulence is physically quenched off. As a result, a number of studies have employed effective shear-viscous models in order to capture the effects of magneto-turbulent motion in the remnant of BNS mergers. An approach to handle this problem has been suggested with the use of general-relativistic large-eddy simulations (LES) in pure hydrodynamics. This method maps effects from numerical calculations with high resolution to simulations with lower resolution, which would otherwise disappear in an implicit filtering procedure (Radice 2017; Radice et al. 2018a,c; Radice 2020). The same method has been systematically extended to the full set GRMHD equations to study the amplification of the magnetic field shortly after merger (Viganò et al. 2020; Aguilera-Miret et al. 2020). In this way, it was shown that by considering the subgrid-scale model for the induction equation only, and suitably increasing (well above the expected value of order one) the phenomenological coefficients associated with the LES terms, magnetic-field strengths comparable to an high-resolution direct simulation can be achieved.

While the robustness and universality – i.e., their effectiveness to capture multi-scale turbu-

lence without expensive fine tuning – remains to be assessed (see [Duez et al. 2020](#), for a careful comparison of momentum transport models for numerical relativity), the inclusion of genuinely dissipative effects already in the general-relativistic hydrodynamics or MHD equations offers the possibility to study a variety of physical phenomena on more robust grounds, where the much larger computational costs can be compensated by the use of high-order methods [see, e.g., [Radice & Rezzolla 2012](#); [Most et al. 2019](#) for standard finite-volume/difference methods, and [Fambri et al. 2018](#); [Hebert et al. 2018](#) for more advanced approaches]. A first attempt in the direct solution of the dissipative hydrodynamics equations has been made by [Duez et al. \(2004\)](#), who has performed simulations in full general relativity of a differentially rotating star, although employing an acausal formulation of the equations of dissipative hydrodynamics. More recently, [Shibata et al. \(2017\)](#) and [Fujibayashi et al. \(2018\)](#) have employed an incomplete but causal viscous model motivated by the work of [Israel & Stewart \(1979\)](#) to assess the effects of turbulence in long-term evolutions of BNS-merger remnants. In this way, it was found that viscous effects can significantly change the amount and composition of the matter outflow from BNS mergers, altering the electromagnetic signal and nucleosynthetic yields ([Baiotti & Rezzolla 2017](#); [Shibata & Hotokezaka 2019](#); [Burns 2020](#)). These studies, together with the prospects suggested by the microphysical investigations of [Alford et al. \(2018\)](#) clearly motivate a more comprehensive and mathematically complete use of general-relativistic hydrodynamics of non-perfect fluids to study BNS mergers.

Although the use of dissipative relativistic-hydrodynamics effects has only just started in the modelling of BNS mergers, this is not the case when describing the special-relativistic evolution of hot and dense strongly interacting matter created in heavy-ion collisions (HICs). In this case, a vast literature has been developed on the optimal way to model dissipative effects in such collisions (see, e.g., [Romatschke & Romatschke 2019](#); [Busza et al. 2018](#), for some recent reviews) and extract from them the imprint of the shear and bulk viscosity to be compared with the experimental data ([Bernhard et al. 2019](#)).

We here make use of the bulk of knowledge developed to model numerically dissipative effects in HICs (see [McNelis et al. 2021](#) for some very recent overview) to propose a comprehensive description of general-relativistic dissipative hydrodynamics (GRDHD) to be used for modelling dissipative effects in BNS mergers. In particular, we propose a complete formulation of the equations of GRDHD based on a second-order description of relativistic dissipative effects and cast them into a 3+1 split of spacetime, in which they can then be coupled to the solution of the Einstein equations. More specifically, we choose the equations first derived by [Israel \(1976\)](#), in the notation of [Hiscock & Lindblom \(1983\)](#) (from now on denoted as **HL83**), to serve as our reference

second-order theory. We discuss the properties of this formulation and provide a comprehensive comparison with other and equivalent formulations of relativistic dissipative hydrodynamics that have been proposed and employed in the literature. In addition, we discuss the implementation of this formulation in the general-relativistic magnetohydrodynamics code BHAC, where it is subject to a number of tests in special and general relativity.

The structure of the paper is as follows. In Section 2 we first provide a brief review of relativistic dissipative hydrodynamics mostly to recall definitions and conventions, while Section 3 is dedicated to the presentation of the set of the **HL83** equations in a general four-dimensional manifold. Extending the work of Peitz & Appl (1997) and Peitz & Appl (1999), in Section 4 we derive a 3+1 decomposed version of **HL83**, including all source terms and gradients of fluid variables, which are separately listed in Section 4.3, such that the coupling to a numerical-relativity code becomes possible. In Section 5 we use this formulation to implement a simplified version for bulk viscosity in the GRMHD code BHAC (Porth et al. 2017) and perform tests in special relativity in Section 6. As a first but rigorous test in general relativity, we consider in Section 7 the problem of stationary, spherically symmetric viscous accretion onto a black hole. We conclude this work in Section 8, where we also comment on future developments. A number of Appendices is also used to provide additional information on the currently available second-order descriptions of relativistic dissipative effects and the differences among them. In addition, details are provided on the numerical solution of the viscous accretion problem, which is less trivial than may appear at first sight.

Unless stated otherwise, we use geometrised units, where the speed of light  $c = 1$  and the gravitational constant  $G = 1$ . Greek letters denote spacetime indices, i.e.,  $\mu = 0, 1, 2, 3$ , while Roman letters cover spatial indices only, i.e.,  $i = 1, 2, 3$ . Also, we make use of Einstein's summation convention and choose the metric signature to be  $(-, +, +, +)$ . Bold symbols such as  $\mathbf{g}$  refer to tensors of generic rank while the symbol  $\nabla$  denotes the covariant derivative with respect to  $\mathbf{g}$  and we use the following definitions for the components of a symmetric and antisymmetric rank-2 tensor:  $T^{(\mu\nu)} := \frac{1}{2}(T^{\mu\nu} + T^{\nu\mu})$ ,  $T^{[\mu\nu]} := \frac{1}{2}(T^{\mu\nu} - T^{\nu\mu})$ .

## 2 RELATIVISTIC DISSIPATIVE HYDRODYNAMICS: A BRIEF OVERVIEW

A large portion of the theory of relativistic dissipative hydrodynamics dates back to the 70's and is both vast and somewhat confusing, with multiple formulations having been produced, often without a clear demarcation or obvious guidance on which formulation may be seen as the most robust.

For this reason, we use this Section to provide a very brief overview of the formulations proposed and of the terminology that has been introduced with them (see also [Rezzolla & Zanotti 2013](#), for a more systematic introduction to the relativistic hydrodynamics of non-perfect fluids). We start by recalling that, in general, one distinguishes between first-order and second-order relativistic dissipative hydrodynamics. “*First-order*” theories are relativistic extensions of the Navier-Stokes (NS) equations, in which the dissipative quantities are directly related to first-order gradients of the primary fluid variables appearing in perfect-fluid hydrodynamics, such as e.g., pressure, rest-mass density and fluid velocity<sup>1</sup>. However, already early on ([Hiscock & Lindblom 1985](#); [Hiscock & Lindblom 1987](#)), it was shown that a large class of first-order theories suffer from instability as well as acausal behaviour due to their parabolic nature ([Hiscock & Lindblom 1985](#); [Hiscock & Lindblom 1987](#); [Denicol et al. 2008a](#)). Because of this drawback, “*second-order*” theories were developed, which extend first-order theories by including terms of second order in quantities which describe deviations from perfect-fluid hydrodynamics. On the one hand, these are dissipative currents like bulk-viscosity pressure, heat current (also referred to as heat flux) or shear-stress tensor. On the other hand, these are gradients of the primary fluid variables, which are in principle independent from the dissipative currents.

While this can be done in different ways, here we focus on three conceptually rather different approaches. The first approach was suggested originally by [Israel \(1976\)](#) and it extends the definition of the entropy current by all terms of second order in the dissipative currents allowed by symmetry. The second-law of thermodynamics then leads to relaxation-type equations for the dissipative currents (see also [Hiscock & Lindblom 1983](#); [Muronga 2004](#); [Jaiswal et al. 2013](#)).

The second approach, instead, adds to the definitions of the dissipative currents all terms of second order in gradients of the primary fluid variables that are allowed by symmetry. This approach follows in spirit that of a systematic gradient expansion and was first suggested by [Baier et al. \(2008\)](#). Unfortunately, second-order (spatial) gradients usually destroy the hyperbolic nature of a partial differential equation. To counter this problem and obtain a hyperbolic formulation – that can therefore be solved numerically – an amendment to the gradient expansion was proposed by [Baier et al. \(2008\)](#), where gradients of primary fluid variables were replaced by dissipative currents, using the first-order Navier-Stokes relation. This effectively leads to a resummation of gradients and, ultimately, to relaxation-type equations for the dissipative currents.

<sup>1</sup> The large majority of these works concentrate on single-fluid scenarios, but valuable work has been done also when considering dissipative hydrodynamics of multi-fluids [see, e.g., [Carter 1989](#); [Andersson & Comer 2015](#), but also [Andersson & Comer 2020](#) for a recent review].

Finally, the third approach considers hydrodynamics as an effective theory in the long-wavelength, low-frequency limit of an underlying microscopic theory. Taking kinetic theory for the latter, it is possible to derive hydrodynamics from the relativistic Boltzmann equation and the method of moments (Israel & Stewart 1979; Betz et al. 2009; Denicol et al. 2012a,b; Jaiswal 2013). This approach leads to an infinite system of coupled equations of motion for the moments of the deviation of the single-particle distribution function from local equilibrium. In particular, Denicol et al. (2012b) have proposed a systematic power-counting scheme in Knudsen and inverse Reynolds numbers that allows for a truncation of the infinite set of moment equations at an arbitrary order in these quantities (Denicol et al. 2014).

The stability and causality of second-order theories has been studied in a series of works. In particular, stability and causality were analysed in a linear regime using the rest frame of the fluid (Hiscock & Lindblom 1983), with the extension to a moving frame in the case of either bulk viscosity (Denicol et al. 2008a), or of shear viscosity (Pu et al. 2010). In this way, it was found that stability implies causality and vice-versa, but only if the relaxation times are larger than a certain timescale. These studies were recently extended to include heat flow (Brito & Denicol 2020) and a magnetic field (Biswas et al. 2020).

While most of these works have considered either a flat Minkowski background or a fixed curved background, recent works have studied the coupling of Einstein equations to second-order dissipative hydrodynamics. This has been done by Bemfica et al. (2019b) when considering only the effects of bulk viscosity and by Bemfica et al. (2020) when including also shear viscosity. These second-order formulations – that are shown to be causal and to admit unique solutions under rather reasonable conditions – effectively pave the way for applications in numerical relativity and hence for the modelling of BNS mergers.

We conclude this overview Section by remarking that it has become clear recently that the unstable and acausal behaviour of first-order theories discussed above is actually related to the particular choice of rest frame of the fluid, for instance the particle frame proposed by Eckart (1940) or the energy-density frame proposed by Landau & Lifshitz (2004). As a result, new causal and stable formulations of first-order theories have been found by choosing different rest frames (Van & Biro 2012; Disconzi et al. 2017; Bemfica et al. 2019a; Kovtun 2019; Houtt & Kovtun 2020; Taghinavaz 2020). The prospects of using these theories, that are in principle easier to solve numerically, are very good but no concrete application to HICs or BNS mergers has been presented yet.

### 3 A COMPREHENSIVE FORMULATION OF GRDHD VIA THE ENTROPY CURRENT

In this Section, we briefly review the phenomenological approach to second-order GRDHD leading to the **HL83** formulation in a generic four-dimensional manifold. The first assumption made is that the rest-mass<sup>2</sup> current  $J^\mu$  and the energy-momentum tensor  $T^{\mu\nu}$  continue to provide a valid description for fluids which are out of thermodynamical equilibrium. Fluids in such an off-equilibrium state show dissipative effects, which characterize them as non-perfect fluids. Hereafter, we will distinguish perfect fluids from generic (non-perfect) fluids, by using the lower index “PF”.

The conservation of rest mass (or some associated conserved number density), energy, and momentum, is expressed by the five conservation equations

$$\nabla_\mu J^\mu = 0, \quad (1)$$

$$\nabla_\mu T^{\mu\nu} = 0, \quad (2)$$

where  $J^\mu = J^\mu_{\text{PF}}$  and  $T^{\mu\nu} = T^{\mu\nu}_{\text{PF}}$ . These equations can be complemented by one equation of state (EOS) of the form

$$e_{\text{PF}} = e_{\text{PF}}(\rho_{\text{PF}}, p_{\text{PF}}), \quad (3)$$

so that perfect fluids need only five independent variables to be described. However, under more general conditions, i.e., for non-perfect fluids,  $J^\mu$  and  $T^{\mu\nu} = T^{\nu\mu}$  contain 14 independent variables. The physical meaning of the nine additional degrees of freedom for non-perfect fluids can be made transparent in a tensor decomposition with respect to the fluid velocity  $u^\mu$ . Choosing the Eckart frame (Eckart 1940; Rezzolla & Zanotti 2013), where  $u^\mu$  is the velocity of the flow of rest mass, the energy-momentum tensor reads

$$T^{\mu\nu} = e u^\mu u^\nu + (p + \Pi) h^{\mu\nu} + 2q^{(\mu} u^{\nu)} + \pi^{\mu\nu}, \quad (4)$$

while  $J^\mu = \rho u^\mu$  maintains the form of the rest-mass current of a perfect fluid, where  $\rho$  is the rest-mass density.

In Eq. (4),  $e$  and  $p + \Pi$  are the energy density and the total isotropic pressure,  $\Pi$  is the bulk-viscosity pressure and  $h^{\mu\nu} := g^{\mu\nu} + u^\mu u^\nu$  is the projector orthogonal to  $u^\mu$ , respectively. Furthermore,  $q^\mu$  is the heat current, which is orthogonal to the fluid four-velocity, i.e.,  $q^\mu u_\mu = 0$ . Finally,  $\pi^{\mu\nu}$  is the shear-stress tensor with the following properties: it is symmetric  $\pi^{\mu\nu} = \pi^{\nu\mu}$ , purely spatial  $\pi^{\mu\nu} u_\mu = 0$ , and trace-free  $\pi^\mu{}_\mu = 0$ .

<sup>2</sup> Hereafter we will always refer to rest mass as this is a quantity normally conserved in simulations of neutron stars. However, the rest mass here can be replaced by any other conserved charge, e.g., baryon number.



As a result of the additional degrees of freedom, the bulk-viscosity pressure adds one, the heat current three and the shear-stress tensor five independent variables to the non-perfect energy-momentum tensor. Note that one can define the temperature  $T$  and the baryon chemical potential  $\mu$  by matching the energy density  $e$  and the number density  $n$  to the corresponding values of a fictitious equilibrium state, i.e.,  $e = e_{\text{pf}}$ ,  $n = n_{\text{pf}}$ , such that  $p = p_{\text{pf}}$ , and then from well-known thermodynamical relations also  $T$  and  $\mu$ , can be determined from the EOS (3):

$$\frac{1}{T} = \left( \frac{\partial s}{\partial e} \right)_n, \quad \mu = -T \left( \frac{\partial s}{\partial n} \right)_e, \quad s = \frac{e + p - \mu n}{T}, \quad (5)$$

where  $s$  denotes the entropy density. We also remark that in the Landau frame (Landau & Lifshitz 2004; Rezzolla & Zanotti 2013), where the fluid four-velocity is the timelike eigenvector of the energy-momentum tensor, the heat current is absent in the tensor decomposition (4), but its three independent degrees of freedom reappear in the form of a diffusion current as part of the non-perfect rest-mass current.

Hereafter, we will make use of the Eckart frame because it is more intuitive to relate the fluid four-velocity to the motion of particles in astrophysical scenarios. In contrast to that, one often chooses the Landau frame in the context of heavy-ion collisions, because baryon chemical potentials are typically small in the center of the collision zone.

To close the system (1)–(2), we need therefore nine additional equations which determine the evolution of the dissipative currents  $\Pi$ ,  $q^\mu$  and  $\pi^{\mu\nu}$ . Following Israel (1976) and Hiscock & Lindblom (1983), such relations are obtained by ensuring the positivity of entropy production. The entropy current depends quadratically on the dissipative currents and reads:

$$\mathcal{S}^\mu = su^\mu + \frac{q^\mu}{T} - (\beta_0 \Pi^2 + \beta_1 q_\alpha q^\alpha + \beta_2 \pi_{\alpha\beta} \pi^{\alpha\beta}) \frac{u^\mu}{2T} + \alpha_0 \frac{\Pi q^\mu}{T} + \alpha_1 \frac{q_\alpha \pi^{\alpha\mu}}{T}, \quad (6)$$

where the physical meaning of the coefficients  $\alpha_0, \alpha_1, \beta_0, \beta_1, \beta_2$  will become clear below. From the second law of thermodynamics, i.e.

$$\nabla_\mu \mathcal{S}^\mu \geq 0, \quad (7)$$



the following set of constitutive equations is obtained

$$\tau_{\Pi} \dot{\Pi} = \Pi_{\text{NS}} - \Pi - \frac{1}{2} \zeta \Pi T \nabla_{\mu} \left( \frac{\tau_{\Pi} u^{\mu}}{\zeta T} \right) + \alpha_0 \zeta \nabla_{\mu} q^{\mu} + \gamma_0 \zeta T q^{\mu} \nabla_{\mu} \left( \frac{\alpha_0}{T} \right), \quad (8)$$

$$\begin{aligned} \tau_q \dot{q}^{(\mu)} &= q_{\text{NS}}^{\mu} - q^{\mu} - \frac{1}{2} \kappa T^2 q^{\mu} \nabla_{\nu} \left( \frac{\tau_q u^{\nu}}{\kappa T^2} \right) \\ &+ \kappa T \left[ \alpha_0 \nabla^{(\mu)} \Pi + \alpha_1 \nabla_{\nu} \pi^{\nu(\mu)} \right. \\ &\left. + (1 - \gamma_0) \Pi T \nabla^{(\mu)} \left( \frac{\alpha_0}{T} \right) + (1 - \gamma_1) T \pi^{\mu\nu} \nabla_{\nu} \left( \frac{\alpha_1}{T} \right) \right], \end{aligned} \quad (9)$$

$$\tau_{\pi} \dot{\pi}^{(\mu\nu)} = \pi_{\text{NS}}^{\mu\nu} - \pi^{\mu\nu} - \frac{1}{2} \eta T \pi^{\mu\nu} \nabla_{\lambda} \left( \frac{\tau_{\pi} u^{\lambda}}{\eta T} \right) + 2\alpha_1 \eta \nabla^{(\mu} q^{\nu)} + 2\gamma_1 \eta T q^{(\mu} \nabla^{\nu)} \left( \frac{\alpha_1}{T} \right), \quad (10)$$

where we have introduced two new coefficients,  $\gamma_0$  and  $\gamma_1$ , whose existence is due to the ambiguity when factoring out the terms which involve the products  $\Pi q^{\mu}$  and  $q_{\alpha} \pi^{\alpha\mu}$ . Also, note in the expressions above the introduction of an operator we will often employ, i.e., the “comoving derivative”  $\dot{\mathbf{A}} := (\mathbf{u} \cdot \nabla) \mathbf{A} = u^{\mu} \nabla_{\mu} \mathbf{A}$ , where  $\mathbf{A}$  can be an arbitrary tensor field. The comoving derivative is naturally accompanied by “relaxation times” for the bulk-viscosity pressure, the heat current, and shear-stress tensor, that are respectively defined as

$$\tau_{\Pi} := \beta_0 \zeta, \quad \tau_q := \beta_1 \kappa T, \quad \tau_{\pi} := 2\beta_2 \eta. \quad (11)$$

where  $\zeta$  is the bulk viscosity,  $\kappa$  the heat conductivity, and  $\eta$  the shear viscosity, respectively. All of these coefficients are by definition non-negative and they essentially set the timescales over which non-equilibrium effects act to push the equations of GRDHD towards the NS solution. Clearly, an inviscid fluid has zero relaxation times.

A physically intuitive interpretation of the bulk-viscosity pressure, of the heat current, and of the shear-stress tensor comes from the naive extensions of the non-relativistic NS equations (Landau & Lifshitz 2004), which leads to the NS expressions of these quantities as<sup>3</sup>

$$\Pi_{\text{NS}} = -\zeta \Theta, \quad (12)$$

$$q_{\text{NS}}^{\mu} = -\kappa T \left( \nabla^{(\mu)} \ln T + a^{\mu} \right), \quad (13)$$

$$\pi_{\text{NS}}^{\mu\nu} = -2\eta \sigma^{\mu\nu}, \quad (14)$$

Furthermore, we define  $b^{(\mu)} := h^{\mu}_{\nu} b^{\nu}$  the projection of an arbitrary vector  $b^{\mu}$  onto the direction orthogonal to  $u^{\mu}$ , while  $b^{(\mu\nu)} := (h_{\alpha}^{(\mu} h^{\nu)}_{\beta} - \frac{1}{3} h^{\mu\nu} h_{\alpha\beta}) b^{\alpha\beta}$  denotes the symmetric and trace-free

<sup>3</sup> Note that after using the conservation equations (2) for perfect fluids, which read  $m n h a^{\mu} = -\nabla^{(\mu)} p$  – where  $h$  is the specific enthalpy and  $m$  the rest mass of the particles constituting the fluid – and using the Gibbs-Duhem relation, i.e.,  $dp = s dT + n d\mu$ , the NS value of the heat current (13) can also be approximated by the expression  $q_{\text{NS}}^{\mu} = (\kappa T^2 / m h) \nabla^{(\mu)} (\mu / T)$ . This expression is an identity at first order in gradients of primary fluid variables and in dissipative currents in the sense that if higher-order terms would be used in the form of the acceleration, then terms of order  $\mathcal{O}_{2K}$  or  $\mathcal{O}_{2R}$  or  $\mathcal{O}_{RK}$  would appear [see Eq. (A4) in Appendix A for the definitions of the symbols  $\mathcal{O}_{2K}$ ,  $\mathcal{O}_{2R}$  and  $\mathcal{O}_{RK}$ ].

projection of an arbitrary tensor  $b^{\mu\nu}$  orthogonal  $u^\mu$ . It is then easy to show that when the entropy current contains only first-order dissipative currents, i.e.,  $\beta_0 = \beta_1 = \beta_2 = \alpha_0 = \alpha_1 = 0$ , then (Rezzolla & Zanotti 2013):

$$\Pi = \Pi_{\text{NS}} , \quad (15)$$

$$q^\mu = q_{\text{NS}}^\mu , \quad (16)$$

$$\pi^{\mu\nu} = \pi_{\text{NS}}^{\mu\nu} , \quad (17)$$

As anticipated in Sec. 2, Eqs. (15)–(17) are acausal and fall into the class of equations investigated by Hiscock & Lindblom (1985) that were shown to be unstable around hydrostatic equilibrium states.

## 4 GENERAL-RELATIVISTIC DISSIPATIVE HYDRODYNAMICS: 3+1 CONSERVATIVE FORMULATION

We next derive a general-relativistic 3+1 flux-conservative (or simply “conservative”) formulation of the dissipative-hydrodynamics Eqs. (8) – (10) so as to provide a comprehensive and complete way of including causal dissipative effects in general-relativistic calculations.

### 4.1 3+1 decomposition of spacetime

As customary in the so-called 3+1 decomposition of spacetime, we decompose the four-dimensional manifold such that notions of time and space reappear. This can be achieved by foliating spacetime in terms of a set of non-intersecting spacelike hypersurfaces. On each hypersurface a unit timelike four-vector field  $\mathbf{n}$  can be defined such that  $\mathbf{n}$  is normal to its corresponding hypersurface. As we have  $n_\mu n^\mu = -1$ , its trajectory can also be interpreted as a reference observer, called “normal” or “Eulerian” observer. In this way, it is possible represent physical laws in terms of projections either parallel or orthogonal to  $\mathbf{n}$ . For a detailed description of this formalism we refer to Alcubierre (2008),ourgoulhon (2012), and Rezzolla & Zanotti (2013).

The generic line-element in a 3+1 decomposition can be written as

$$ds^2 = -(\alpha^2 - \beta_i \beta^i) dt^2 + 2\beta_i dx^i dt + \gamma_{ij} dx^i dx^j , \quad (18)$$

where  $\alpha$  is the so-called lapse function, the purely spatial vector  $\beta$ , i.e.,  $\beta^\mu = (0, \beta^i)^T$ , is the shift vector and  $\gamma_{ij}$  denotes the components of the purely spatial metric  $\gamma$ , defined as

$$\gamma_{\mu\nu} := g_{\mu\nu} + n_\mu n_\nu , \quad (19)$$

which acts as the projection operator onto spatial hypersurfaces. Note that the following identities

then follow:  $\beta_i := \gamma_{ij}\beta^j$ ,  $\sqrt{-g} = \alpha\sqrt{\gamma}$ , where  $g := \det(g_{\mu\nu})$  and  $\gamma := \det(\gamma_{ij})$ . The components of  $\mathbf{n}$  and its dual are given by:

$$n^\mu = \frac{1}{\alpha}(1, -\beta^i)^T, \quad n_\mu = (-\alpha, 0, 0, 0). \quad (20)$$

Having a timelike unit four-vector  $\mathbf{n}$ , we can use it to decompose any tensor into a part that is parallel ( $\parallel$ ) and perpendicular ( $\perp$ ) to it. We start from the four-velocity  $u^\mu$ , which can then be written as:

$$u^\mu = u_\parallel^\mu + u_\perp^\mu := (-n_\nu u^\nu)n^\mu + \gamma^\mu{}_\nu u^\nu = W(n^\mu + v^\mu), \quad (21)$$

where  $W := (1 - v_i v^i)^{-1/2}$  is the Lorentz factor and  $v^\mu := (0, v^i)^T$  the fluid velocity measured by the normal observer. Analogously, we can decompose the heat current  $q^\mu$  and the shear-stress tensor  $\pi^{\mu\nu}$  into components relative to  $\mathbf{n}$ :

$$q^\mu = q_\parallel^\mu + q_\perp^\mu := (-n_\nu q^\nu)n^\mu + \gamma^\mu{}_\nu q^\nu, \quad (22)$$

$$\begin{aligned} \pi^{\mu\nu} &= \pi_\parallel^{\mu\nu} + \pi_\times^{\mu\nu} + \pi_\times^{\nu\mu} + \pi_\perp^{\mu\nu} \\ &:= (n_\alpha n_\beta \pi^{\alpha\beta}) n^\mu n^\nu + (-n_\alpha \gamma^\nu{}_\beta \pi^{\alpha\beta}) n^\mu + (-n_\beta \gamma^\mu{}_\alpha \pi^{\alpha\beta}) n^\nu + \gamma^\mu{}_\alpha \gamma^\nu{}_\beta \pi^{\alpha\beta}. \end{aligned} \quad (23)$$

Additionally, since the time components of the parallel projections are effectively scalar functions, we treat them as such after the following definitions

$$\dot{q} := -n_\mu q^\mu, \quad (24)$$

$$\dot{\pi} := n_\mu n_\nu \pi^{\mu\nu}, \quad (25)$$

$$\dot{\pi}^\lambda := -n_\mu \gamma^\lambda{}_\nu \pi^{\mu\nu}. \quad (26)$$

Note that the parallel and perpendicular components are not independent and indeed the following identities can be obtained and will be used hereafter

$$\dot{q} = v_i q_\perp^i, \quad \dot{\pi}^i = v_j \pi_\perp^{ij}, \quad \dot{\pi} = v_i \dot{\pi}^i = \pi_\perp^i{}_i. \quad (27)$$

Note that expressions (27) imply that the knowledge of  $q_\perp^i$  and  $\pi_\perp^{ij}$  suffices to fully reconstruct  $q^\mu$  and  $\pi^{\mu\nu}$  if the fluid three-velocity  $v^i$  and the full metric  $g_{\mu\nu}$  is known.

The projections (27) turn out to be helpful in the 3+1 decomposition of the non-perfect energy-momentum tensor (4)

$$T^{\mu\nu} = E n^\mu n^\nu + S^\mu n^\nu + S^\nu n^\mu + S^{\mu\nu}, \quad (28)$$

where

$$E := n_\mu n_\nu T^{\mu\nu} = (e + p + \Pi) W^2 + 2\dot{q}W - (p + \Pi - \dot{\pi}) , \quad (29)$$

$$S^\mu := -n_\nu \gamma^\mu{}_\alpha T^{\alpha\nu} = (e + p + \Pi) W^2 v^\mu + W \left( \dot{q}v^\mu + q_\perp{}^\mu \right) + \dot{\pi}^\mu , \quad (30)$$

$$S^{\mu\nu} := \gamma^\mu{}_\alpha \gamma^\nu{}_\beta T^{\alpha\beta} = (e + p + \Pi) W^2 v^\mu v^\nu + W \left( q_\perp{}^\mu v^\nu + q_\perp{}^\nu v^\mu \right) + (p + \Pi) \gamma^{\mu\nu} + \pi_\perp{}^{\mu\nu} , \quad (31)$$

are: the energy density, the momentum density, and the purely spatial part of the energy-momentum tensor, respectively. Additionally, we will make use of the acceleration of the normal observer and the extrinsic curvature given by

$$\hat{a}^\mu := n^\nu \nabla_\nu n^\mu = \gamma^{\mu\nu} \partial_\nu \ln \alpha , \quad (32)$$

$$K_{\mu\nu} := -\frac{1}{2} \mathcal{L}_n \gamma_{\mu\nu} = -\gamma_\mu{}^\lambda \nabla_\lambda n_\nu = -\nabla_\mu n_\nu - n_\mu \hat{a}_\nu , \quad (33)$$

respectively, where  $\mathcal{L}_n$  denotes the Lie derivative along  $\mathbf{n}$ . Finally, we recall two important four-dimensional tensor identities that will be useful later on to obtain a flux-conservative formulation for the conservation of rest mass (1) and energy-momentum (2), namely,

$$\nabla_\mu J^\mu = \frac{\partial_\mu (\sqrt{-g} J^\mu)}{\sqrt{-g}} , \quad (34)$$

$$\nabla_\mu T^{\mu\nu} = g^{\nu\lambda} \left[ \frac{\partial_\mu (\sqrt{-g} T^\mu{}_\lambda)}{\sqrt{-g}} - \frac{1}{2} T^{\alpha\beta} \partial_\lambda g_{\alpha\beta} \right] . \quad (35)$$

## 4.2 3+1, flux-conservative formulation of HL83: general expressions

We next rewrite the full set of general-relativistic dissipative hydrodynamics, i.e., Eqs. (1), (2), and (8) – (10), and which essentially represent the equations of the **HL83** formulation, in a 3+1 flux-conservative form. We start by recalling that a system of partial differential equations is said to be flux-conservative (or simply “conservative”) if it can be written as

$$\partial_t \mathbf{U} + \partial_i \mathbf{F}^i(\mathbf{U}) = \mathbf{S} , \quad (36)$$

where  $\mathbf{U}$  is the “state vector”,  $\mathbf{F}^i$  are the “flux vectors” and  $\mathbf{S}$  is the “source vector”. Employing now Eq. (34) it is possible to rewrite Eq. (1) as

$$\partial_t (\sqrt{\gamma} D) + \partial_i [\sqrt{\gamma} D (\alpha v^i - \beta^i)] = 0 , \quad (37)$$

where  $D := \rho \alpha u^t = \rho W$  is the conserved rest mass. Similarly, we use equations (28) and (35) to obtain a flux-conservative form of the equations for the conservation of energy and momentum (2)

$$\partial_t (\sqrt{\gamma} S_j) + \partial_i [\sqrt{\gamma} (\alpha S^i{}_j - \beta^i S_j)] = \sqrt{\gamma} \left( \frac{1}{2} \alpha S^{ik} \partial_j \gamma_{ik} + S_i \partial_j \beta^i - E \partial_j \alpha \right) , \quad (38)$$

$$\partial_t [\sqrt{\gamma} (E - D)] + \partial_i \{ \sqrt{\gamma} [\alpha (S^i - v^i D) - \beta^i (E - D)] \} = \sqrt{\gamma} (\alpha S^{ij} K_{ij} - S^j \partial_j \alpha) . \quad (39)$$

Note that we use  $E - D$  rather than simply  $E$  in equation (39) because the conservation of  $E - D$  is more accurate than that of  $E$  only. Comparing Eqs. (36)–(39) we can now read off the components of  $\mathbf{U}$ ,  $\mathbf{F}^i$  and  $\mathbf{S}$  corresponding to the conservation equations. We will write them down explicitly in the next Section, after we have reformulated the constitutive equations (8)–(10) in conservative form. In order to do this, we consider the evolution equation for the heat current (9) as an example and extend the treatment to the other equations afterwards. We start with the term

$$\dot{q}^{(\mu)} = h^\mu{}_\nu u^\lambda \nabla_\lambda q^\nu = u^\lambda \nabla_\lambda q^\mu - a_\nu q^\nu u^\mu, \quad (40)$$

where we used the fact that  $\mathbf{q} \cdot \mathbf{u} = 0$  and have introduced the kinematic acceleration  $\mathbf{a}$  – not to be confused with the acceleration of normal observers  $\hat{\mathbf{a}}$  – with components  $a^\mu := u^\lambda \nabla_\lambda u^\mu$ . Our goal is to obtain evolution equations in a conservative form for state variables that are orthogonal to  $\mathbf{n}$ . Thus, we project Eq. (40) by multiplying with  $\gamma^i{}_\mu$ :

$$\begin{aligned} \gamma^i{}_\mu \dot{q}^{(\mu)} &= u^\lambda \nabla_\lambda q_\perp^i - q^\mu u^\nu \nabla_\nu \gamma^i{}_\mu - a_\nu q^\nu \gamma^i{}_\mu u^\mu \\ &= u^\lambda \partial_\lambda q_\perp^i - \mathcal{G}_q^i - \mathcal{H}_q^i, \end{aligned} \quad (41)$$

where, upon using Eq. (33) and the definition of the covariant derivative, we have introduced the new quantities

$$\mathcal{G}_q^i := \frac{W}{\alpha} (K_{kj} v^k - \hat{a}_j) q_\perp^j \beta^i + \dot{q} W v_j K^{ij} - \dot{q} W \hat{a}^i - \frac{W}{\alpha} \Gamma^i{}_{0j} q_\perp^j - \frac{W}{\alpha} \Gamma^i{}_{jk} q_\perp^j V^k, \quad (42)$$

$$\mathcal{H}_q^i := (a_{\perp j} q_\perp^j - \hat{a} \dot{q}) W v^i. \quad (43)$$

The right-hand sides of Eqs. (42) and (43) also contain other new quantities, namely, the “*coordinate velocity*”  $V^j := u^j/u^t = \alpha v^j - \beta^j$  and the 3+1 split of the kinematic acceleration  $a^\mu := a_\parallel^\mu + a_\perp^\mu = \hat{a} n^\mu + a_\perp^\mu$ , whose explicit components are given by

$$a_\perp^i = A^i + W \Lambda^i - 2W^2 v_j K^{ij}, \quad (44)$$

$$\hat{a} = v_i a_\perp^i = v_i A^i + W v_i \Lambda^i - 2W^2 v_i v_j K^{ij}, \quad (45)$$

with

$$A^i := W v^j D_j (W v^i), \quad (46)$$

$$\Lambda^i := \frac{1}{\alpha} (\partial_t - \mathcal{L}_\beta) W v^i + W \hat{a}^i. \quad (47)$$

and  $D_j$  being the fully spatial part of the covariant derivative  $\nabla$ , i.e.,  $D_j v^i := \partial_j v^i + {}^3\Gamma^i{}_{jk} v^k$ , where  ${}^3\Gamma^i{}_{jk}$  represent the Christoffel symbols related to the three-metric  $\gamma$  (see [Gourgoulhon 2012](#); [Rezzolla & Zanotti 2013](#), for details)

$${}^3\Gamma^i{}_{jk} := \frac{1}{2} \gamma^{il} (\partial_j \gamma_{lk} + \partial_j \gamma_{lk} - \partial_l \gamma_{jk}). \quad (48)$$

Note that the vector  $\mathcal{G}_q^i$  captures the influence of the choice of spacetime foliation as well as the curvature of spacetime itself on the transport of heat on each hypersurface. On the other hand, the tensor  $\mathcal{H}_q^i$  is a correction term that arises from the projection operator  $h^\mu_\nu$ , which ensures that heat transport occurs always orthogonal to  $u$ . Notice that at this point  $\mathcal{G}_q^i$  and  $\mathcal{H}_q^i$  are not fully 3+1 decomposed due to  $\hat{a}$ ,  $\hat{q}$  and the corresponding Christoffel symbols not yet being fully split. Their full 3+1 decomposition will be given in Section 4.3 as both terms belong to the source terms.

Now we exploit the continuity equation in the form (34) in order to modify the first term on the right-hand side of Eq. (41):

$$\alpha\sqrt{\gamma}\rho u^\lambda\partial_\lambda q_\perp^i = \partial_\lambda (\alpha\sqrt{\gamma}\rho q_\perp^i u^\lambda) = \partial_t (\sqrt{\gamma}Dq_\perp^i) + \partial_j (\sqrt{\gamma}DV^j q_\perp^i). \quad (49)$$

Using this equation, as well as Eq. (41), and projecting Eq. (9) with  $\gamma^i_\mu$ , we obtain

$$\begin{aligned} \partial_t (\sqrt{\gamma}Dq_\perp^i) + \partial_j (\sqrt{\gamma}DV^j q_\perp^i) &= \frac{\alpha\sqrt{\gamma}D}{\tau_q W} \left\{ \gamma^i_\mu q_{\text{NS}}^\mu - q_\perp^i - \frac{1}{2}\kappa T^2 q_\perp^i \nabla_\nu \left( \frac{\tau_q u^\nu}{\kappa T^2} \right) \right. \\ &\quad + \kappa T \left[ \alpha_0 \gamma^i_\mu \nabla^{(\mu} \Pi + \alpha_1 \gamma^i_\mu \nabla_\nu \pi^{\nu(\mu} \right. \\ &\quad \left. \left. + (1 - \gamma_0) \Pi T \gamma^i_\mu \nabla^{(\mu} \left( \frac{\alpha_0}{T} \right) + (1 - \gamma_1) T \gamma^i_\mu \pi^{\mu\nu} \nabla_\nu \left( \frac{\alpha_1}{T} \right) \right] \right. \\ &\quad \left. + \tau_q [\mathcal{G}_q^i + \mathcal{H}_q^i] \right\}. \end{aligned} \quad (50)$$

Proceeding in a similar way, we find that the projected version of equation (10) is given by

$$\begin{aligned} \partial_t (\sqrt{\gamma}D\pi_\perp^{ij}) + \partial_k (\sqrt{\gamma}DV^k \pi_\perp^{ij}) &= \frac{\alpha\sqrt{\gamma}D}{\tau_\pi W} \left\{ \gamma^i_\mu \gamma^j_\nu \pi_{\text{NS}}^{\mu\nu} - \pi_\perp^{ij} - \frac{1}{2}\eta T \pi_\perp^{ij} \nabla_\lambda \left( \frac{\tau_\pi u^\lambda}{\eta T} \right) \right. \\ &\quad + 2\alpha_1 \eta \gamma^i_\mu \gamma^j_\nu \nabla^{(\mu} q^{\nu)} + 2\gamma_1 \eta T \gamma^j_\nu \gamma^i_\mu q^{(\mu} \nabla^{\nu)} \left( \frac{\alpha_1}{T} \right) \\ &\quad \left. + \tau_\pi [\mathcal{G}_\pi^{ij} + \mathcal{H}_\pi^{ij}] \right\}, \end{aligned} \quad (51)$$

with

$$\begin{aligned} \mathcal{G}_\pi^{ij} &:= \frac{W}{\alpha} (K_{lk} v^l - \hat{a}_k) (\pi_\perp^{ki} \beta^j + \pi_\perp^{kj} \beta^i) + W v_l (K^{li} \hat{\pi}^j + K^{lj} \hat{\pi}^i) - W (\hat{a}^i \hat{\pi}^j + \hat{a}^j \hat{\pi}^i), \\ &\quad - \frac{W}{\alpha} (\Gamma^i_{0k} \pi_\perp^{kj} + \Gamma^j_{0k} \pi_\perp^{ki}) - \frac{W}{\alpha} (\Gamma^i_{kl} \pi_\perp^{kj} V^l + \Gamma^j_{kl} \pi_\perp^{ki} V^l), \end{aligned} \quad (52)$$

$$\mathcal{H}_\pi^{ij} := W a_{\perp k} (\pi_\perp^{ki} v^j + \pi_\perp^{kj} v^i) - W \hat{a} (\hat{\pi}^i v^j + \hat{\pi}^j v^i). \quad (53)$$

Finally, since the bulk-viscosity pressure  $\Pi$  is a scalar quantity, there are no projections that have to be performed in order to write a 3+1 split version of Eq. (8):

$$\begin{aligned} \partial_t (\sqrt{\gamma}D\Pi) + \partial_i (\sqrt{\gamma}DV^i \Pi) &= \frac{\alpha\sqrt{\gamma}D}{\tau_\Pi W} \left[ \Pi_{\text{NS}} - \Pi - \frac{1}{2}\zeta \Pi T \nabla_\mu \left( \frac{\tau_\Pi u^\mu}{\zeta T} \right) \right. \\ &\quad \left. + \alpha_0 \zeta \nabla_\mu q^\mu + \gamma_0 \zeta T q^\mu \nabla_\mu \left( \frac{\alpha_0}{T} \right) \right]. \end{aligned} \quad (54)$$

In summary, Eqs. (37)–(39), (50), (51) and (54) can be combined into the flux-conservative

form (36), with the following expressions for the quantities  $U$ ,  $F^i$  and  $S$

$$U = \sqrt{\gamma} \begin{pmatrix} D \\ S^j \\ E - D \\ D\Pi \\ Dq_{\perp}^j \\ D\pi_{\perp}^{jk} \end{pmatrix} = \sqrt{\gamma} \begin{pmatrix} \rho W \\ (e + p + \Pi) W^2 v^j + W (\dot{q} v^j + q_{\perp}^j) + \dot{\pi}^j \\ (e + p + \Pi) W^2 + 2\dot{q}W - (p + \Pi - \dot{\pi}) - \rho W \\ \rho W \Pi \\ \rho W q_{\perp}^j \\ \rho W \pi_{\perp}^{jk} \end{pmatrix}, \quad (55)$$

$$F^i = \sqrt{\gamma} \begin{pmatrix} DV^i \\ \alpha S^i_j - \beta^i S_j \\ \alpha (S^i - v^i D) - \beta^i (E - D) \\ DV^i \Pi \\ DV^i q_{\perp}^j \\ DV^i \pi_{\perp}^{jk} \end{pmatrix}, \quad (56)$$

$$S = \sqrt{\gamma} \begin{pmatrix} 0 \\ \frac{1}{2} \alpha S^{ik} \partial_j \gamma_{ik} + S_i \partial_j \beta^i - E \partial_j \alpha \\ \alpha S^{ij} K_{ij} - S^j \partial_j \alpha \\ (\alpha D / \tau_{\Pi} W) (\Pi_{\text{NS}} - \Pi + \Delta_{\Pi}) \\ (\alpha D / \tau_{\text{q}} W) (\gamma^j_{\mu} q_{\text{NS}}^{\mu} - q_{\perp}^j + \Delta_{\text{q}}^j + \tau_{\text{q}} \mathcal{G}_{\text{q}}^j + \tau_{\text{q}} \mathcal{H}_{\text{q}}^j) \\ (\alpha D / \tau_{\pi} W) (\gamma^j_{\mu} \gamma^k_{\nu} \pi_{\text{NS}}^{\mu\nu} - \pi_{\perp}^{jk} + \Delta_{\pi}^{jk} + \tau_{\pi} \mathcal{G}_{\pi}^{jk} + \tau_{\pi} \mathcal{H}_{\pi}^{jk}) \end{pmatrix}, \quad (57)$$



where we have introduced the following new quantities:

$$\Delta_{\Pi} := -\frac{1}{2}\zeta\Pi T\nabla_{\mu}\left(\frac{\tau_{\Pi}u^{\mu}}{\zeta T}\right) + \alpha_0\zeta\nabla_{\mu}q^{\mu} + \gamma_0\zeta Tq^{\mu}\nabla_{\mu}\left(\frac{\alpha_0}{T}\right), \quad (58)$$

$$\begin{aligned} \Delta_q^j := & -\frac{1}{2}\kappa T^2 q_{\perp}^j \nabla_{\nu}\left(\frac{\tau_q u^{\nu}}{\kappa T^2}\right) + \kappa T \left[ \alpha_0 \gamma^j_{\mu} \nabla^{\langle\mu} \Pi + \alpha_1 \gamma^j_{\mu} \nabla_{\nu} \gamma^j_{\mu} \nabla^{\langle\mu} \left(\frac{\alpha_0}{T}\right) \right. \\ & \left. + (1 - \gamma_1) T \gamma^j_{\mu} \pi^{\mu\nu} \nabla_{\nu} \left(\frac{\alpha_1}{T}\right) \right], \end{aligned} \quad (59)$$

$$\Delta_{\pi}^{jk} := -\frac{1}{2}\eta T \pi_{\perp}^{jk} \nabla_{\lambda} \left(\frac{\tau_{\pi} u^{\lambda}}{\eta T}\right) + 2\alpha_1 \eta \gamma^j_{\mu} \gamma^k_{\nu} \nabla^{\langle\mu} q^{\nu\rangle} + 2\gamma_1 \eta T \gamma^k_{\mu} \gamma^j_{\nu} q^{\langle\mu} \nabla^{\nu\rangle} \left(\frac{\alpha_1}{T}\right). \quad (60)$$

The evolution equations (36) for the fifteen components of the state vector (57), with fluxes given by the vectors (56), and source terms (57) represent the 3+1 flux-conservative formulation of the **HL83** system.

A few considerations are worth making at this point. First, although the whole solution of the set of partial differential equations becomes computationally more expensive, the conversion from the conserved to the primitive variables does not gain complexity, at least not beyond what is already encountered in GRMHD. We recall that such a conversion, which needs to be performed numerically at each grid cell and on each timelevel of the solution, requires the solution of a set of nonlinear equations to obtain the values of the primitive variables from the newly computed conserved ones. Fortunately, the extension of the set of equations in GRDHD does not require new root-finding steps to obtain the ten new primitive variables, i.e.,  $\Pi$ ,  $q_{\perp}^i$ ,  $\pi_{\perp}^{ij}$ , as these are related algebraically with the corresponding components of the state vector  $\mathbf{U}$ . Second, the way in which the new conversion from the conserved to the primitive variables differs from the perfect-fluid case is in the appearance of the three-velocities  $v^i$  in the definitions of the conserved variables, i.e., Eqs. (29) – (30), as well as in the contractions with the projected dissipative currents  $q_{\perp}^i$  and  $\pi_{\perp}^{ij}$ . While the latter are related algebraically with the corresponding conserved variables, the three-velocity  $v^i$  still requires a numerical root-finding and hence a continuous update in the root-finding process. Ultimately, this leads to a numerical matrix inversion or additional root-finding steps in the conversion when compared to the perfect-fluid case. Second, a different choice of second-order theory will only change the explicit expressions for  $\Delta_{\Pi}$ ,  $\Delta_q^j$  and  $\Delta_{\pi}^{jk}$ . Stated differently,  $\Delta_{\Pi}$ ,  $\Delta_q^j$  and  $\Delta_{\pi}^{jk}$  contain off-equilibrium contributions that are not captured by simple relaxation-type equations and typically contain contributions that are of second and even higher order. A few examples of other second-order GRDHD equations are presented in Appendix A, where we compare **HL83** to other dissipative-hydrodynamics formulations. Finally, we remark that the sources for the dissipative quantities in Eqs. (57) are not yet fully 3+1 decomposed and their explicit expressions will be presented in the following Section.

### 4.3 3+1, flux-conservative formulation of HL83: source terms

As mentioned above, in order to provide complete expressions for the 3+1, flux-conservative formulation of Eqs. (36) we need to obtain right-hand sides that only contain fully spatial quantities, both for the ordinary variables – i.e.,  $\rho, p, v^i, \alpha, \beta^i, \gamma_{ij}, K_{ij}$ , as well as their spatial (partial) derivatives – and for the dissipative ones, as well as their temporal and spatial (partial and covariant) derivatives – i.e.,  $\Pi, q_\perp^i$  and  $\pi_\perp^{ij}$ .

To accomplish this second goal, we need to project the corresponding evolution equations – and corresponding right-hand sides – onto spatial hypersurfaces via the metric  $\gamma$ . However, since many terms in the source terms involve covariant derivatives [cf., Eqs. (58)–(60)], the resulting 3+1 decomposed expressions are inevitably very complicated and lengthy, so that it is difficult to reconstruct the origin of the various source terms. To avoid this, and hence make the calculations more transparent and easy to follow, we collect the relevant source terms in the following classes:

1. *Intrinsically spatial terms.* These are terms containing only quantities which are originally defined on a spatial hypersurface, i.e.,  $\rho, p, v^i, \Pi, q_\perp^i$  and  $\pi_\perp^{ij}$ , as well as spatial partial or covariant derivatives of these quantities. Also part of this class are terms proportional to  $\gamma_{ij}$  and its spatial partial derivatives. We have marked these terms in **green**.
2. *Terms not containing the extrinsic curvature  $K_{ij}$ .* These are terms involving temporal derivatives, spatial derivatives involving  $\alpha$  or  $\beta^i$ , as well as terms containing projections parallel to the unit normal  $\mathbf{n}$ , e.g.,  $\hat{q}$ . We have marked these terms in **orange**.
3. *Terms containing the extrinsic curvature  $K_{ij}$ .* These are terms linear in the extrinsic curvature, its trace,  $K := \gamma_{ij} K^{ij}$ , but not containing spatial derivatives of  $K_{ij}$ . We have marked these terms in **light blue**.

However, before proceeding to this classification, we recall a number of useful identities that will be exploited in the derivation of the source terms and that are associated to gradients of the fluid four-velocity; in doing so we are following in part the convention introduced by Peitz & Appl (1997, 1999). We first recall that the covariant derivative of the four-velocity can be decomposed in terms of tensors that describe its properties in terms of changes in volumes, shape and vorticity, i.e., as (Rezzolla & Zanotti 2013)

$$\nabla_\mu u_\nu = \omega_{\mu\nu} + \sigma_{\mu\nu} + \frac{1}{3}\Theta h_{\mu\nu} - u_\mu a_\nu, \quad (61)$$

where  $\Theta$  is the “*expansion*” and is defined as

$$\Theta := \nabla_\mu u^\mu = \vartheta + \textcolor{orange}{\Lambda} - \textcolor{lightblue}{KW}, \quad (62)$$

and where we have introduced

$$\vartheta := D_i (W v^i) = \frac{\partial_i (\sqrt{\gamma} W v^i)}{\sqrt{\gamma}}, \quad (63)$$

$$\Lambda := \frac{1}{\alpha} (\partial_t - \mathcal{L}_\beta) W + W v_i \hat{a}^i. \quad (64)$$

Similarly, the “*shear tensor*” can be written as:

$$\sigma^{\mu\nu} := \nabla^{\langle\mu} u^{\nu\rangle} = \dot{\sigma} n^\mu n^\nu + \dot{\sigma}^\mu n^\nu + \dot{\sigma}^\nu n^\mu + \sigma_\perp^{\mu\nu}, \quad (65)$$

where

$$\sigma_\perp^{ij} = \gamma^i_\mu \gamma^j_\nu \nabla^{\langle\mu} u^{\nu\rangle} = \Sigma^{ij} + \Lambda^{ij} - W \mathcal{K}^{ij}, \quad (66)$$

with

$$\Sigma^{ij} := \frac{1}{2} [D^i (W v^j) + D^j (W v^i)] + \frac{1}{2} W (A^i v^j + A^j v^i) - \frac{1}{3} (\gamma^{ij} + W^2 v^i v^j) \vartheta, \quad (67)$$

$$\Lambda^{ij} := \frac{1}{2} W^2 (\Lambda^i v^j + \Lambda^j v^i) - \frac{1}{3} \Lambda (\gamma^{ij} + W^2 v^i v^j), \quad (68)$$

$$\mathcal{K}^{ij} := K^{ij} + W^2 v_k (K^{ik} v^j + K^{jk} v^i) - \frac{1}{3} K (\gamma^{ij} + W^2 v^i v^j), \quad (69)$$

$$\dot{\sigma}^i = v_j \sigma_\perp^{ij}, \quad (70)$$

$$\dot{\sigma} = \gamma_{ij} \sigma_\perp^{ij} = \sigma_\perp^i{}_i. \quad (71)$$

Finally, the “*kinematic vorticity*” has the form:

$$\omega^{\mu\nu} := \nabla^{[\mu} u^{\nu]} + u^{[\mu} a^{\nu]} = \dot{\omega}^\mu n^\nu - \dot{\omega}^\nu n^\mu + \omega_\perp^{\mu\nu}, \quad (72)$$

where

$$\omega_\perp^{ij} = \Omega^{ij} - \frac{1}{2} W^2 (\Lambda^i v^j - \Lambda^j v^i) + W^3 v_k (K^{ik} v^j - K^{jk} v^i), \quad (73)$$

with

$$\Omega^{ij} := D^{[i} W v^{j]} - W A^{[i} v^{j]}, \quad \text{and} \quad \dot{\omega}^i := -n_\nu \gamma^i_\lambda \omega^{\lambda\nu} = v_j \omega_\perp^{ij}. \quad (74)$$

#### 4.3.1 Sources for the evolution of the bulk-viscosity pressure

Listed below are all the spatial source terms [6-th component of the vector  $\mathbf{S}$  in (57)] appearing in the evolution equation for the bulk-viscosity pressure, i.e.,  $\partial_t (\sqrt{\gamma} D\Pi) = \dots$

$$\Pi_{\text{NS}} = -\zeta (\vartheta + \Lambda - KW), \quad (75)$$

$$\begin{aligned} \frac{1}{2}\zeta\Pi T\nabla_\mu \left( \frac{\tau_\Pi u^\mu}{\zeta T} \right) &= \frac{1}{2}\tau_\Pi \Pi \vartheta + \frac{1}{2}\zeta\Pi TW v^i \partial_i \left( \frac{\tau_\Pi}{\zeta T} \right) \\ &+ \frac{1}{2}\tau_\Pi \Pi \Lambda + \frac{\zeta\Pi TW}{2\alpha} (\partial_t - \mathcal{L}_\beta) \left( \frac{\tau_\Pi}{\zeta T} \right) - \frac{1}{2}\tau_\Pi \Pi WK, \end{aligned} \quad (76)$$

$$\nabla_\mu q^\mu = D_i q_\perp^i + \frac{1}{\alpha} (\partial_t - \mathcal{L}_\beta) \dot{q} + \hat{a}_i q_\perp^i - \dot{q} K, \quad (77)$$

$$q^\mu \nabla_\mu \left( \frac{\alpha_0}{T} \right) = q_\perp^i \partial_i \left( \frac{\alpha_0}{T} \right) + \frac{\dot{q}}{\alpha} (\partial_t - \mathcal{L}_\beta) \left( \frac{\alpha_0}{T} \right). \quad (78)$$

#### 4.3.2 Sources for the evolution of the heat current

Similarly, listed below are all the spatial source terms [components 7-9 in Eq. (57)] appearing in the evolution equation for the components of the perpendicular heat current, i.e.,  $\partial_t (\sqrt{\gamma} Dq_\perp^i) = \dots$

$$\begin{aligned} \gamma^i_\mu q_{\text{NS}}^\mu &= -\kappa T \left[ (\gamma^{ij} + W^2 v^i v^j) \partial_j \ln(T) + A^i \right. \\ &\quad \left. + \frac{W^2}{\alpha} v^i (\partial_t - \mathcal{L}_\beta) \ln(T) + W\Lambda^i - 2W^2 K^i_j v^j \right], \end{aligned} \quad (79)$$

$$\begin{aligned} \frac{1}{2}\kappa T^2 q_\perp^i \nabla_\nu \left( \frac{\tau_q u^\nu}{\kappa T^2} \right) &= \frac{1}{2}\tau_q q_\perp^i \vartheta + \frac{1}{2}\kappa T^2 q_\perp^i W v^j \partial_j \left( \frac{\tau_q}{\kappa T^2} \right) \\ &+ \frac{1}{2}\tau_q q_\perp^i \Lambda + \frac{\kappa T^2 q_\perp^i W}{2\alpha} (\partial_t - \mathcal{L}_\beta) \left( \frac{\tau_q}{\kappa T^2} \right) - \frac{1}{2}\tau_q q_\perp^i WK, \end{aligned} \quad (80)$$

$$\gamma^i_\mu h^{\mu\nu} \nabla_\nu \Pi = (\gamma^{ij} + W^2 v^i v^j) \partial_j \Pi + \frac{W^2}{\alpha} v^i (\partial_t - \mathcal{L}_\beta) \Pi, \quad (81)$$

$$\begin{aligned} \gamma^i_\mu \nabla_\nu \pi^{\nu\langle\mu\rangle} &= D_j \pi_\perp^{ij} + W^2 v^i v_k D_j \pi_\perp^{jk} \\ &- W^2 v^i D_j \dot{\pi}^j + \frac{1}{\alpha} (\partial_t - \mathcal{L}_\beta) \dot{\pi}^i - \hat{a}_j \pi_\perp^{ij} - \dot{\pi} \hat{a}^i \\ &+ W v^i \left[ \frac{v_k}{\alpha} (\partial_t - \mathcal{L}_\beta) \dot{\pi}^k - \frac{1}{\alpha} (\partial_t - \mathcal{L}_\beta) \dot{\pi} - 3\hat{a}_j \dot{\pi}^j - \dot{\pi} v_k \hat{a}^k \right] \\ &- 2K^i_j \dot{\pi}^j - W^2 v^i (2K_{jk} \dot{\pi}^j v^k - K_{jk} \pi_\perp^{jk} - \dot{\pi} K), \end{aligned} \quad (82)$$

$$(1 - \gamma_0) \Pi T \gamma^i_\mu \nabla^{\langle\mu\rangle} \left( \frac{\alpha_0}{T} \right) = (1 - \gamma_0) \Pi T \left[ \gamma^{ij} \partial_j + W^2 v^i v^j \partial_j + \frac{W^2}{\alpha} (\partial_t - \mathcal{L}_\beta) \right] \left( \frac{\alpha_0}{T} \right), \quad (83)$$

$$(1 - \gamma_1) T \gamma^i_\mu \pi^{\mu\nu} \nabla_\nu \left( \frac{\alpha_1}{T} \right) = (1 - \gamma_1) T \pi_\perp^{ij} \partial_j \left( \frac{\alpha_1}{T} \right) + \frac{(1 - \gamma_1) T \dot{\pi}^i}{\alpha} (\partial_t - \mathcal{L}_\beta) \left( \frac{\alpha_1}{T} \right), \quad (84)$$

$$\mathcal{H}_q^i = W v^i \left( A_j q_{\perp}^j + W \Lambda_j q_{\perp}^j - \dot{q} W v_j \Lambda^j - \dot{q} v_j A^j - 2W^2 K_{kj} q_{\perp}^k v^j + 2\dot{q} W^2 K_{kj} v^k v^j \right), \quad (85)$$

$$\mathcal{G}_q^i = -W^3 \Gamma_{jk}^i q_{\perp}^j v^k - \dot{q} W \hat{a}^i - \frac{W}{\alpha} q_{\perp}^j \partial_j \beta^i + \dot{q} W v_j K^{ij} + W K_{jk}^i q_{\perp}^j. \quad (86)$$

#### 4.3.3 Sources for the evolution of the shear-stress tensor

Finally, listed below are all the spatial source terms [components 10-15 in Eq. (57)] appearing in the evolution equation for the components of the perpendicular shear-stress tensor, i.e.,  $\partial_t \left( \sqrt{\gamma} D \pi_{\perp}^{ij} \right) = \dots$

$$\gamma^i_{\mu} \gamma^j_{\nu} \pi_{\text{NS}}^{\mu\nu} = -2\eta \left( \Sigma^{ij} + \Lambda^{ij} - W K^{ij} \right), \quad (87)$$

$$\begin{aligned} \frac{1}{2} \eta T \pi_{\perp}^{ij} \nabla_{\lambda} \left( \frac{\tau_{\pi} u^{\lambda}}{\eta T} \right) &= \frac{1}{2} \tau_{\pi} \pi_{\perp}^{ij} \vartheta + \frac{1}{2} \eta T \pi_{\perp}^{ij} W v^i \partial_i \left( \frac{\tau_{\pi}}{\eta T} \right) \\ &\quad + \frac{1}{2} \tau_{\pi} \pi_{\perp}^{ij} \Lambda + \frac{\eta T \pi_{\perp}^{ij} W}{2\alpha} (\partial_t - \mathcal{L}_{\beta}) \left( \frac{\tau_{\pi}}{\eta T} \right) - \frac{1}{2} \tau_{\pi} \pi_{\perp}^{ij} W K, \end{aligned} \quad (88)$$

$$\begin{aligned} \gamma^i_{\mu} \gamma^j_{\nu} \nabla^{\langle \mu} q^{\nu \rangle} &= D^{(i} q_{\perp}^{j)} + \frac{1}{2} W^2 v^i \left( v^k D_k q_{\perp}^j + v_k D^j q_{\perp}^k \right) + \frac{1}{2} W^2 v^j \left( v^k D_k q_{\perp}^i + v_k D^i q_{\perp}^k \right) \\ &\quad - W^2 v^i v^j A_k q_{\perp}^k - \frac{1}{3} (\gamma^{ij} + W^2 v^i v^j) (D_k q_{\perp}^k - A_k q_{\perp}^k) \\ &\quad + \frac{1}{2} W^2 v^i \left[ \frac{1}{\alpha} (\partial_t - \mathcal{L}_{\beta}) q_{\perp}^j + \dot{q} \hat{a}^j - \gamma^{jk} \partial_k \dot{q} \right] \\ &\quad + \frac{1}{2} W^2 v^j \left[ \frac{1}{\alpha} (\partial_t - \mathcal{L}_{\beta}) q_{\perp}^i + \dot{q} \hat{a}^i - \gamma^{ik} \partial_k \dot{q} \right] \\ &\quad - W^2 v^i v^j (W \Lambda_k q_{\perp}^k - \dot{q} W \Lambda_k v^k - \dot{q} A_k v^k) \\ &\quad - \frac{1}{3} (\gamma^{ij} + W^2 v^i v^j) \left[ \frac{1}{\alpha} (\partial_t - \mathcal{L}_{\beta}) \dot{q} - W \Lambda_k q_{\perp}^k + \hat{a}_k q_{\perp}^k + \dot{q} W \Lambda_k v^k + \dot{q} A_k v^k \right] \\ &\quad - \dot{q} K^{ij} - \dot{q} W^2 v_k (K^{ik} v^j + K^{jk} v^i) + 2W^4 v^i v^j K_{kl} (q_{\perp}^k v^l - \dot{q} v^k v^l) \\ &\quad + \frac{1}{3} (\gamma^{ij} + W^2 v^i v^j) K_{kl} (2\dot{q} W^2 v^k v^l - 2W^2 q_{\perp}^k v^l + \dot{q} \gamma^{kl}), \end{aligned} \quad (89)$$

$$\begin{aligned} \gamma^j_{\nu} \gamma^i_{\mu} q^{\langle \mu} \nabla^{\nu \rangle} \left( \frac{\alpha_1}{T} \right) &= \left\{ \frac{1}{2} \left[ q_{\perp}^i \left( \gamma^{jk} \partial_k + W^2 v^j v^k \partial_k + \frac{W^2 v^j}{\alpha} (\partial_t - \mathcal{L}_{\beta}) \right) \right. \right. \\ &\quad \left. \left. + q_{\perp}^j \left( \gamma^{ik} \partial_k + W^2 v^i v^k \partial_k + \frac{W^2 v^i}{\alpha} (\partial_t - \mathcal{L}_{\beta}) \right) \right] \right. \\ &\quad \left. - \frac{1}{3} (\gamma^{ij} + W^2 v^i v^j) \left( q_{\perp}^k \partial_k + \frac{\dot{q}}{\alpha} (\partial_t - \mathcal{L}_{\beta}) \right) \right\} \left( \frac{\alpha_1}{T} \right), \end{aligned} \quad (90)$$

$$\begin{aligned}
\mathcal{H}_\pi^{ij} = & W A_k \left( \pi_\perp^{ik} v^j + \pi_\perp^{jk} v^i \right) \\
& + W^2 \Lambda_k \left( \pi_\perp^{ik} v^j + \pi_\perp^{jk} v^i \right) - W \left( v_l A^l + W v_l \Lambda^l \right) \left( \hat{\pi}^i v^j + \hat{\pi}^j v^i \right) \\
& - 2W^3 K_{lk} v^l \left( \pi_\perp^{ik} v^j + \pi_\perp^{jk} v^i \right) + 2W^3 K_{lk} v^l v^k \left( \hat{\pi}^i v^j + \hat{\pi}^j v^i \right), \tag{91}
\end{aligned}$$

$$\begin{aligned}
\mathcal{G}_\pi^{ij} = & -W v^l \left( {}^3\Gamma_{kl}^i \pi_\perp^{kj} + {}^3\Gamma_{kl}^j \pi_\perp^{ki} \right) \\
& - W \left( \hat{\pi}^i \hat{a}^j + \hat{\pi}^j \hat{a}^i \right) - \frac{W}{\alpha} \left( \pi_\perp^{ik} \partial_k \beta^j + \pi_\perp^{jk} \partial_k \beta^i \right) \\
& + W v^l \left( K_l^i \hat{\pi}^j + K_l^j \hat{\pi}^i \right) + W \left( K^i_l \pi_\perp^{lj} + K^j_l \pi_\perp^{li} \right). \tag{92}
\end{aligned}$$

#### 4.3.4 Corollary: explicit expressions for the Christoffel symbols

As a corollary to the lengthy expressions provided above and as a way to help in the actual numerical implementation of Eqs. (36), we provide below also the explicit expressions for the Christoffel symbols appearing in the source terms (57)

$$\Gamma_{00}^0 = \partial_t \ln \alpha + \hat{a}_i \beta^i - \frac{1}{\alpha} K_{ij} \beta^i \beta^j, \tag{93}$$

$$\Gamma_{0i}^0 = \hat{a}_i - \frac{1}{\alpha} K_{ij} \beta^j, \tag{94}$$

$$\Gamma_{ij}^0 = -\frac{1}{\alpha} K_{ij}, \tag{95}$$

$$\begin{aligned}
\Gamma_{00}^i = & \partial_t \beta^i - \beta^i \partial_t \ln \alpha + \beta^j \partial_j \beta^i + \frac{1}{2} \gamma^{ij} \partial_j \alpha^2 - \beta^i \beta^j \partial_j \ln \alpha + {}^3\Gamma_{jk}^i \beta^j \beta^k \\
& - 2\alpha K_{ij} \beta^j + \frac{1}{\alpha} \beta^i K_{jk} \beta^j \beta^k, \tag{96}
\end{aligned}$$

$$\Gamma_{0j}^i = \partial_j \beta^i - \beta^i \partial_j \ln \alpha + {}^3\Gamma_{jk}^i \beta^k + \frac{1}{\alpha} \beta^i K_{jk} \beta^k - \alpha K_{ij}, \tag{97}$$

$$\Gamma_{jk}^i = {}^3\Gamma_{jk}^i + \frac{1}{\alpha} \beta^i K_{jk}. \tag{98}$$

In summary, the 3+1 flux-conservative formulation of the general-relativistic Eqs. (36), combined with the explicit components Eqs. (55)–(57) and Eqs. (58)–(60), provides a complete and ready-to-use set of equations for the numerical evaluation of dissipative effects in special-relativistic simulations of colliding heavy ions as well as in general-relativistic simulations of compact objects. In Appendix A we provide a detailed comparison of the system presented here with that of other formulations (see Table A2).

## 5 GENERAL-RELATIVISTIC DISSIPATIVE HYDRODYNAMICS: NUMERICAL IMPLEMENTATION

After having presented a fully general, causal, 3+1 split, and flux-conservative formulation of the equations of general-relativistic dissipative hydrodynamics, i.e., Eqs. (36) with explicit components (55)–(57), we now turn to a numerical implementation and the strategy that needs to be developed when these equations have to be cast within an already developed GRHD or GRMHD code. For simplicity, but also because the issues that will be discussed below would apply also for more complicated (and complete) forms of the equations, hereafter we concentrate on a reduced set after neglecting the heat current and the shear-stress tensor in Eqs. (55)–(57), i.e., after setting  $q_\perp^i = 0 = \pi_\perp^{ij}$ <sup>4</sup>. Furthermore, we will also assume that the off-equilibrium contributions to the source terms are very small, i.e.,  $\Delta_\Pi \simeq 0$ , or, equivalently, that  $\Pi$  relaxes towards its NS-value only, ignoring corrections coming from terms of order higher than one in Knudsen number. As a result, the evolution equation for the bulk-viscosity pressure (54) reduces to

$$\partial_t (\sqrt{\gamma} D \Pi) + \partial_i (\sqrt{\gamma} D V^i \Pi) = \frac{\alpha \sqrt{\gamma} D}{\tau_\Pi W} (\Pi_{\text{NS}} - \Pi) = -\frac{\alpha \sqrt{\gamma} D}{\tau_\Pi W} [\zeta (\vartheta + \mathcal{A} - KW) + \Pi], \quad (99)$$

which is a relaxation-type equation, describing the evolution of the bulk-viscosity pressure such that causality is not violated and stability is guaranteed.

The specific implementation discussed here refers to the one made within the Black Hole Accretion Code BHAC (Porth et al. 2017). The code, which solves the equations of GRMHD by means of a finite-volume approach and high-resolution shock-capturing (HRSC) methods, assumes a stationary but curved background, and it has been employed in a number of studies of accretion onto supermassive black holes (Mizuno et al. 2018; Event Horizon Telescope Collaboration et al. 2019; Olivares et al. 2020). Of course, in our present implementation all of the electromagnetic fields are set to zero so that the various terms in Eqs. (36) reduce to

$$U = \sqrt{\gamma} \begin{pmatrix} D \\ S_j \\ E - D \\ D \Pi \end{pmatrix} = \sqrt{\gamma} \begin{pmatrix} \rho W \\ (e + p + \Pi) W^2 v_j \\ (e + p + \Pi) W^2 - (p + \Pi) - \rho W \\ \rho W \Pi \end{pmatrix}, \quad (100)$$

<sup>4</sup> Note that setting to zero the spatial components of the heat current and of the shear-stress tensor implies that also the time components are zero [cf., Eq. (27)].



$$\mathbf{F}^i = \sqrt{\gamma} \begin{pmatrix} V^i D \\ \alpha S^i_j - \beta^i S_j \\ \alpha(S^i - v^i D) - \beta^i(E - D) \\ V^i D \Pi \end{pmatrix}, \quad (101)$$

$$\mathbf{S} = \sqrt{\gamma} \begin{pmatrix} 0 \\ \frac{1}{2} \alpha S^{ik} \partial_j \gamma_{ik} + S_i \partial_j \beta^i - E \partial_j \alpha \\ \frac{1}{2} S^{ik} \beta^j \partial_j \gamma_{ik} + S_i^j \partial_j \beta^i - S^j \partial_j \alpha \\ -(\alpha D / \tau_{\Pi} W) [\zeta (\vartheta + \Lambda - KW) + \Pi] \end{pmatrix}. \quad (102)$$

Clearly, the extra terms that need to be handled in Eqs. (99) either involve divergences or partial derivatives, which can be evaluated using the standard differential operators available within BHAC. For example, the divergence appearing in the term  $\vartheta$  is discretised at second order as

$$\vartheta = \frac{\partial_i(\sqrt{\gamma} W v^i)}{\sqrt{\gamma}} = \frac{\int_V \partial_i(\sqrt{\gamma} W v^i) dV}{\int_V \sqrt{\gamma} dV} = \frac{1}{\Delta V} \sum_{i=1}^3 \left[ (\overline{W} \overline{v}^i \Delta S^i)_{(x^i + \Delta x^i/2)} - (\overline{W} \overline{v}^i \Delta S^i)_{(x^i - \Delta x^i/2)} \right], \quad (103)$$

where the cell volume and cell surfaces are defined respectively as (Porth et al. 2017)

$$\Delta V := \int_V \sqrt{\gamma} dV, \quad \Delta S^i_{(x^i + \Delta x^i/2)} := \int_{(x^i + \Delta x^i/2)} \sqrt{\gamma} dS_i, \quad (104)$$

Each integral is performed over one cell, where the coordinate volume and surface are given by  $dV := dx^1 dx^2 dx^3$  and  $dS_i := s_i dx^{j \neq i} dx^{k \neq i}$ , respectively. The co-vector  $s_i$  is the  $i$ th component of the unit normal with respect to the boundary of the cell. In addition, we calculate the boundary data through averages; for example, given a scalar function  $\phi$ , we compute  $\overline{\phi}_{(x^i + \Delta x^i/2)} := (\phi(x^i + \Delta x^i) + \phi(x^i))/2$ ,  $\overline{\phi}_{(x^i - \Delta x^i/2)} := (\phi(x^i - \Delta x^i) + \phi(x^i))/2$ , and  $\hat{\phi} := \phi(x^i)$ .

Similarly, the volume-averaged partial derivative of a scalar function  $\phi$  (e.g.,  $W$ )

$$\begin{aligned} \partial_i \phi &= \frac{\int_V \sqrt{\gamma} \partial_i \phi dV}{\int_V \sqrt{\gamma} dV} \\ &= \frac{1}{\Delta V} \left[ (\overline{\phi} \Delta S^i)_{(x^i + \Delta x^i/2)} - (\overline{\phi} \Delta S^i)_{(x^i - \Delta x^i/2)} - \hat{\phi} (\Delta S^i)_{(x^i + \Delta x^i/2)} + \hat{\phi} (\Delta S^i)_{(x^i - \Delta x^i/2)} \right]. \end{aligned} \quad (105)$$

Also, the time derivative, such as the one appearing in the term  $\Lambda$ ,  $(\partial_t - \beta^i \partial_i)W$ , is calculated

using central second-order finite differences and a two-step predictor-corrector time evolution

$$(\partial_t W)_c \approx \frac{W(t + \Delta t/2) - W(t - \Delta t/2)}{\Delta t}, \quad (106)$$

where  $W(t - \Delta t/2)$  is saved from the previous timestep and is also used to calculate the predictor step via first-order backward differences  $(\partial_t W)_p \approx [W(t) - W(t - \Delta t/2)]/(\Delta t/2)$ , with  $W(t + \Delta t/2)$  being the Lorentz factor after the predictor step. Finally, for stationary spacetimes, as the one considered here, the trace of the extrinsic curvature can be computed as

$$K = \frac{1}{\alpha} \partial_i \beta^i + \frac{1}{2\alpha} \gamma^{ij} \beta^k \partial_k \gamma_{ij}. \quad (107)$$

Note that the newly evolved bulk-viscosity pressure appears also in the definitions of  $E$ ,  $S_j$ ,  $S^{ij}$ , which need to be suitably updated. Fortunately,  $\Pi$  only appears as a correction to the equilibrium pressure  $p$  in the total pressure of the fluid  $p_t = p + \Pi$ . Therefore, we can rewrite equation (100)–(102) in terms of  $p_t$ , of the total specific enthalpy

$$h_t := h + \frac{\Pi}{\rho} = \frac{e + p + \Pi}{\rho}. \quad (108)$$

and of an effective EOS,  $p_t = p_t(\rho, e, \Pi)$ . As a result, when considering a simple ideal-gas EOS, where the pressure is given by

$$p = (e - \rho)(\gamma - 1), \quad (109)$$

and  $\gamma$  is the adiabatic index, the new effective EOS would then read

$$p_t = (e - \rho)(\gamma - 1) + \Pi, \quad (110)$$

Note that for a generic EOS  $p = p(n, e)$  and particle rest mass  $m$ , the effective sound speed in the presence of bulk viscosity is given by (Bemfica et al. 2019b)

$$c_{s,t}^2 := \left( \frac{\partial p}{\partial e} \right)_n + \frac{1}{mh_t} \left( \frac{\partial p}{\partial n} \right)_e + \frac{\zeta}{\tau_\Pi} \frac{1}{\rho h_t}, \quad (111)$$

where  $n$  is the number density and  $\rho = nm$ . Clearly,  $c_{s,t}^2 > c_s^2$  and so the correct characteristic wave-speeds need to be updated in the presence of bulk viscosity.

As a result, in the code we make use only of the total pressure, of the total specific enthalpy, and of the corresponding sound speed. In other words, in the recovery of the primitive variables from the conserved ones, we perform the following mapping

$$\rho h = \rho + \frac{\gamma}{\gamma - 1} p \quad \rightarrow \quad \rho h_t = \rho + \frac{\gamma}{\gamma - 1} p_t - \frac{1}{\gamma - 1} \Pi, \quad (112)$$

$$p = \frac{\gamma - 1}{\gamma} (\rho h - \rho) \quad \rightarrow \quad p_t = \rho \left( \frac{\gamma - 1}{\gamma} \right) (h_t - 1) + \frac{\Pi}{\gamma}, \quad (113)$$

$$c_s^2 = (\gamma - 1) \frac{h - 1}{h} \quad \rightarrow \quad c_{s,t}^2 = (\gamma - 1) \frac{h_t - 1}{h_t} + \frac{\zeta}{\tau_\Pi} \frac{1}{\rho h_t}. \quad (114)$$

Finally, we note that hereafter we will concentrate on a reduced set of equations, namely, the one obtained after neglecting the heat current and the shear-stress tensor in Eqs. (55)–(57).

## 6 NUMERICAL TESTS: FLAT SPACETIME

In this Section we present the application of the relativistic dissipative-hydrodynamics Eqs. (100)–(102) described in Section 5 to two 1+1-dimensional tests in special relativity. The time integration is carried out explicitly by using a two-step predictor-corrector scheme. Furthermore, we employ the so-called Rusanov (Rusanov 1961) or “TVDLF” flux at the cell boundaries, with wave-speed given by the expression for  $c_{s,t}$  in Eq. (114), although the differences when using instead the expressions for  $c_s$  are at most of the order of 0.6% for the cases considered here. Furthermore, we use the “minmod” reconstruction scheme to compute state variables at cell boundaries (see, e.g., Rezzolla & Zanotti 2013); for more details on the numerical schemes we refer the interested reader to Porth et al. (2017).

### 6.1 Bjorken flow

We first consider the time-honoured Bjorken-flow (Bjorken 1983) when bulk viscosity is present, which still represents a well-known and often-used test in relativistic dissipative hydrodynamics (see, e.g., Del Zanna et al. 2013; Inghirami et al. 2016, 2018) and MHD with transverse magnetic fields (Roy et al. 2015; Pu et al. 2016). We recall that the Bjorken flow is the idealised representation of a one-dimensional, longitudinally boost-invariant motion of a fluid, such as the one produced in an ultrarelativistic collision of two ions.

As usual for the Bjorken-flow scenario, it is convenient to make use of the so-called Milne coordinates, which are given by

$$c\tau := \sqrt{(ct)^2 - z^2}, \quad \eta := \operatorname{artanh}\left(\frac{z}{ct}\right) = \frac{1}{2} \ln \left( \frac{1 + z/(ct)}{1 - z/(ct)} \right), \quad (115)$$

$$t = \tau \cosh \eta, \quad z = c\tau \sinh \eta, \quad (116)$$

where  $\tau$  and  $\eta$  are defined as the proper time and space-time rapidity, respectively. In our setup, the evolution starts at  $\tau = 1 \text{ fm } c^{-1}$  and ends at  $\tau = 15 \text{ fm } c^{-1}$ . The initial conditions are given by

$$(\rho, p, v, \Pi) = (10^{-7} \text{ GeV } c^{-2} \text{ fm}^{-3}, 10.0 \text{ GeV fm}^{-3}, 0.0, 0.0). \quad (117)$$

As the solution does not depend on the coordinate  $\eta$ , all solutions are taken at  $\eta = 0.0$ . Finally, we choose constant values for  $\zeta$  and  $\tau_{\Pi}$ , as reported in the legend of Fig. 1. The analytic solution for

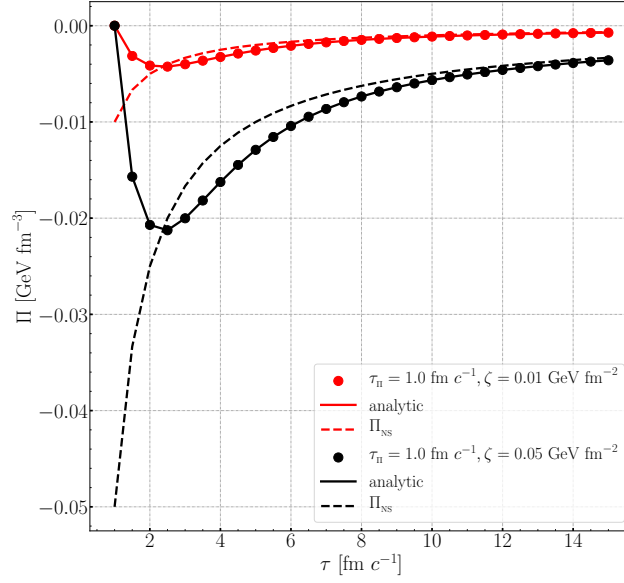


**Figure 1.** Evolution of the bulk-viscosity pressure in a Bjorken flow. Solid lines show the analytic solution, while dashed lines the solution in the NS approximation. Filled circles report instead the numerical solution from BHAC.

this problem is given by

$$\Pi(\tau) = \Pi(\tau_0) \exp[-(\tau - \tau_0)/\tau_\Pi] + \frac{\zeta}{c\tau_\Pi} \exp(-\tau/\tau_\Pi) [\text{Ei}(\tau_0/\tau_\Pi) - \text{Ei}(\tau/\tau_\Pi)] , \quad (118)$$

where  $\text{Ei}(x)$  is the exponential integral function (see, e.g., [Del Zanna et al. 2013](#), for more details).

Figure 1 shows the evolution of the bulk-viscosity pressure  $\Pi$  for the initial data given by Eq. (117) (the changes in the other hydrodynamical quantities are very small and not particularly interesting). As it can be seen, the numerical solutions agree very well with the analytical ones. Also, note that with time,  $\Pi$  converges towards its NS value  $\Pi_{\text{NS}} = -\zeta\Theta = -\zeta/(c\tau)$  (dashed lines in Fig. 1). At any time during the evolution, the relative difference between the analytic and numerical solution is  $10^{-7}$  at most, confirming the correct implementation of the relativistic dissipative-hydrodynamics equations for smooth flows in a flat spacetime. Furthermore, our choices for the pair  $(\zeta, \tau)$  lie well within the range of applicability for the equations of GRDHD.

This can be seen by calculating the effective speed of sound which is given by

$$\frac{c_{s,t}^2}{c^2} = \frac{1}{3} + \frac{\zeta}{c\tau_\Pi} \frac{1}{4p + \Pi} , \quad (119)$$

Requiring causality, i.e.,  $c_{s,t}/c < 1$ , and expressing  $p$  through the perfect-fluid solution  $p(\tau) = p(\tau_0)(\tau_0/\tau)^{4/3}$  we obtain that

$$\tau < \left( \frac{8}{3} c\tau_\Pi \frac{p(\tau_0)}{\zeta} \right)^{3/4} \tau_0 , \quad (120)$$

when  $p \gg |\Pi|$ .

For our choices  $(\zeta, \tau_\Pi) = (0.01 \text{ GeV fm}^{-2}, 1.0 \text{ fm c}^{-1})$  and  $(\zeta, \tau_\Pi) = (0.05 \text{ GeV fm}^{-2}, 1.0 \text{ fm c}^{-1})$

the dimensionless ratio  $|\Pi|/p$  remains below 1% and 5%, respectively, up to the time  $\tau = 400 \text{ fm } c^{-1}$ . Hence, we apply Eq. (120) and find  $\tau < 371 \text{ fm } c^{-1}$  as well as  $\tau < 110 \text{ fm } c^{-1}$ , respectively. Both values agree very well with the ones obtained from the exact solution and lie clearly above the end of the simulation at  $\tau = 15 \text{ fm } c^{-1}$ .

## 6.2 Shock-tube test

We next explore the solution of a shock-tube problem for an ultra-relativistic gas of gluons. While this is a standard 1+1-dimensional test scenario, we here use the same setup implemented by (Bouras et al. 2009a; Gabbana et al. 2020), i.e., we consider the ideal-gas EOS relative to an ultra-relativistic fluid (i.e.,  $\gamma = 4/3$ ). Adopting Cartesian coordinates, the spatial domain ranges from  $x = -3.5 \text{ fm}$  to  $x = 3.5 \text{ fm}$  and the initial discontinuity in pressure and density is located at  $x = 0.0 \text{ fm}$ , while the velocity and bulk-viscosity pressure are assumed to be zero initially. In other words, the initial conditions are given by<sup>5</sup>

$$(T, p, v, \Pi) = \begin{cases} (0.4 \text{ GeV } k_B^{-1}, 5.43 \text{ GeV fm}^{-3}, 0.0, 0.0) & x < 0.0 \text{ fm}, \\ (0.2 \text{ GeV } k_B^{-1}, 0.33 \text{ GeV fm}^{-3}, 0.0, 0.0) & x \geq 0.0 \text{ fm}. \end{cases} \quad (121)$$

On the other hand, we parametrize the bulk-viscosity coefficient  $\zeta$  in terms of the entropy density of the fluid, namely,

$$s = \rho \frac{k_B}{m} \left[ 4 - \ln \left( \frac{\pi^2 \rho}{m d_F T^3} \frac{c^3 \hbar^3}{k_B^3} \right) \right], \quad (122)$$

where  $d_F$  denotes the number of degrees of freedom and is set to 16 for gluons, such that

$$\zeta = \frac{4}{3} \frac{k_B}{c \hbar} \zeta_0 s, \quad (123)$$

The coefficient  $\zeta_0$  is a non-negative number, for which we choose the values  $\zeta_0 = \{0.002, 0.01, 0.1\}$  to obtain a direct comparison with the data from Gabbana et al. (2020). Note that the equations describing the shock-tube problem with bulk viscosity in one dimension take the same form as the corresponding equations with shear viscosity; the latter has been investigated in the work of Bouras et al. (2010), as well as more recently by Gabbana et al. (2020). This leads to the mapping  $\zeta = 4/3 \eta$  between the bulk viscosity employed in this work and the shear viscosity used in Bouras et al. (2010) and Gabbana et al. (2020). Furthermore, to obtain the correct rest-mass density we assume a single-particle rest mass  $m = 0.5 \text{ MeV } c^{-2}$ , so that  $\rho \ll e$ , as required by wanting to consider an ultra-relativistic limit. Finally, the relaxation time used by Gabbana et al. (2020) is

<sup>5</sup> In this Section, to facilitate the comparison with codes designed for describing HICs (Gabbana et al. 2020) we adopt physical units, where  $k_B$  and  $\hbar$  are the Boltzmann and reduced Planck constants, respectively.

given in terms of the bulk viscosity by

$$\tau_{\Pi} = \frac{15}{16} \frac{\zeta}{pc}. \quad (124)$$

The numerical solution of the shock-tube problem at time  $t = 3.2 \text{ fm } c^{-1}$  is shown in Fig. 2, whose upper panels report the behaviour of the pressure normalized to  $p_0 := 5.43 \text{ GeV fm}^{-3}$  (the top right panel is a magnification of the top left panel), while the bottom panels show the solution of the velocity and bulk-viscosity pressure normalized to the fluid pressure. Different lines refer either to solutions obtained with BHAC for different values of  $\zeta_0$ , or to solutions obtained with a relativistic lattice-Boltzmann (RLBM) approach (dashed lines) or to solutions of the relativistic Boltzmann equation via the test-particle (RBMT) approach (dotted lines). Note that the case  $\zeta_0 = 0.002$  is essentially indistinguishable from an inviscid solution with the precision shown in the figure and hence can be taken as the perfect-fluid reference.

Figure 2 highlights how the strong spatial gradients present in the initial conditions tend to be washed out by the presence of bulk viscosity and that this smearing of the discontinuities is larger with increasing bulk viscosity. Note that the wave-pattern of perfect-fluid hydrodynamics – which consists of a rarefaction wave and of a shock wave – can still be clearly identified if the bulk viscosity is not too large, i.e.,  $\zeta_0 \lesssim 0.01$  (see, e.g., the pressure in the upper left panel of Fig. 2). Furthermore, the solution behaviour is in good agreement with the results obtained by using the RLBM approach. However, in the case of high bulk-viscosity, i.e.,  $\zeta_0 = 0.1$ , the wave-pattern of perfect-fluid hydrodynamics is so strongly smeared out that it is difficult to clearly distinguish the rarefaction wave from the shock wave. This is not surprising, since such large values of the bulk viscosity effectively correspond to a regime of large Knudsen number, which is where the hydrodynamical approach – and hence the formation of shock waves – is expected to fail.

Interestingly, and as pointed out by Denicol et al. (2008b) and Bouras et al. (2010), three additional discontinuities are present in the high-viscosity,  $\zeta_0 = 0.1$ , case, two of which can be seen in the upper right panel of Fig. 2, where one is located at the head of the right-propagating shock, while the other near the contact discontinuity of the corresponding inviscid ( $\zeta_0 = 0.002$ ) case<sup>6</sup>. The third additional discontinuity is located at the head of the left-propagating rarefaction fan which is not shown here. However, all discontinuities transition smoothly into the wave-pattern of perfect-fluid hydrodynamics at later times; indeed, the pressure jump located near the contact discontinuity decays to less than 10% of its initial size of  $\simeq 2.4 \text{ GeV fm}^{-3}$  by a time of  $t \simeq 1.8 \text{ fm } c^{-1}$  (see

<sup>6</sup> Obviously the contact discontinuity cannot be seen in the pressure profile, but it is apparent in the rest-mass density profile, which is not shown in Fig. 2.

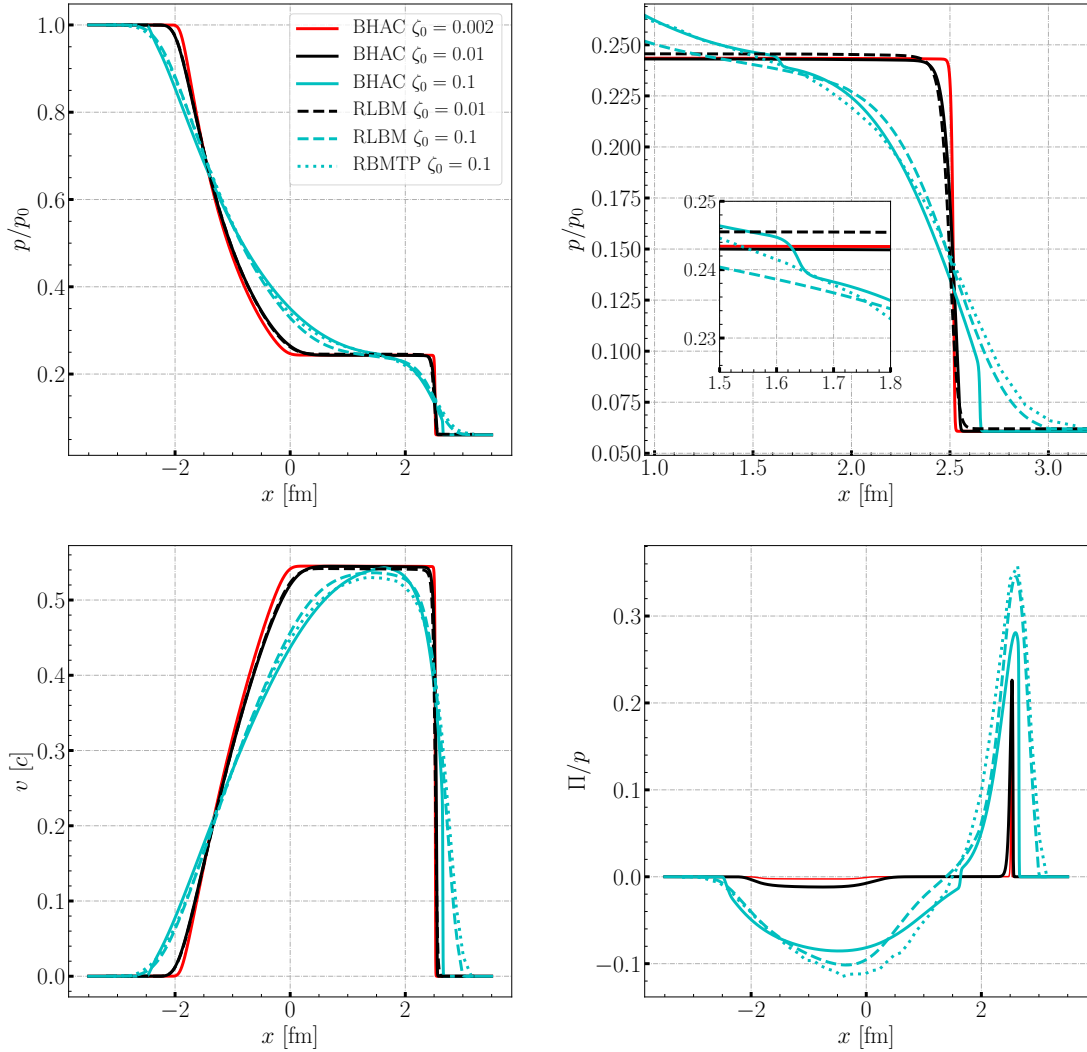


**Figure 2.** Solution of the shock-tube test with initial data given by Eq. (121) and at time  $t = 3.2 \text{ fm } c^{-1}$  for. *Top left:* solution of the pressure normalized to  $p_0 = 5.43 \text{ GeV fm}^{-3}$ ; *top right:* same as in top left but zoomed-in at the shock front; *bottom left:* solution of the three-velocity, *bottom right:* bulk-viscosity pressure normalised to the fluid pressure. In all panels, the solid lines show the results obtained with BHAC, while the dashed or dotted lines present the results using the relativistic lattice-Boltzmann (RLBM) or the test-particle (RBMTP) approach, respectively.

also Bouras et al. 2010, for a more detailed description and a possible explanation). In addition, we find in agreement with Bouras et al. (2009b) that at a time  $t \simeq 3.2 \text{ fm } c^{-1}$  the fluid velocity downstream of the shock front differs by less than 0.5% from the corresponding fluid velocity of the inviscid case. At this point the previously mentioned pressure jump has declined to less than 2% of its original size. Because the new discontinuities are absent in the RLBM (dashed line) and RBMTP (dotted line) solutions, their appearance may well indicate a breakdown of dissipative hydrodynamics for such large viscosities, i.e., for such large Knudsen numbers, which is of course still correctly described by the microscopic approaches RLBM and RBMTP.

In addition, in the high-viscosity case, the BHAC solution underestimates the bulk-viscosity pressure at the head of the right-propagating shock with respect to the values computed with the RLBM or RBMTP approaches (see bottom right panel of Fig. 2). While this may again be due to



the breakdown of the hydrodynamical description, part of the error may also originate from the truncation of the relativistic evolution equation for  $\Pi$  [we recall that we have set  $\Delta_\Pi = 0$  in Eq. (57)]. As remarked by Bouras et al. (2010), the inclusion of additional source terms, as well as of a coupling to a heat current, generally yields a better description of the corresponding dissipative current (see Fig. 10 of Bouras et al. 2010). We expect the same to be true here and hence that a smaller deviation would be obtained with a more sophisticated source term for Eq. (99).

Overall, Fig. 2 shows that our numerical implementation of the relativistic dissipative-hydrodynamics equations leads to solutions that are in very good agreement with the reference solutions obtained by the direct solution of the relativistic Boltzmann equation in regimes that are mildly dissipative, i.e.,  $\zeta_0 \lesssim 0.01$ , and in regimes that are highly dissipative, i.e.,  $\zeta_0 \lesssim 0.1$ . The relative differences remain below 8% for  $p/p_0$  where we only considered the region  $x \in [-2.5, 2.6]$  fm. In this way we exclude rightmost shock wave and the head of the left-propagating rarefaction wave. Due to the fact that the solution obtained by BHAC reaches its unperturbed initial state at lower  $|x|$  than the solutions obtained by RLBM and RBMTP, the relative difference starts growing outside of  $[-2.5, 2.6]$  fm and can reach values close to 45%. Note that this relative difference depends solely on the value of  $p$  in the unperturbed initial states, for instance if the pressure of the right initial state was close to zero then the relative difference would be close to 100% at the rightmost shock wave. Furthermore, we similarly calculate the relative differences for  $\Pi/p$  and obtain values below a maximum of  $\sim 60\%$  which is reached at  $x \sim 2$  fm. Note that  $\Pi/p$  passes through zero such that the corresponding region is excluded, too.

## 7 NUMERICAL TESTS: CURVED SPACETIME

In this Section we present a stationary solution of the spherically symmetric equations of GRDHD in a Schwarzschild spacetime. In the following, we return to using geometrised units. For perfect fluids, the fully general-relativistic solution is known as the so-called “Michel solution” (Michel 1972) and, together with the “Bondi-Hoyle” solution (Bondi 1952), serves as the reference solution for models of accreting nonrotating black holes in spherical symmetry, (see e.g., Nobili et al. 1991, and references therein) as well as serves as a testbed for GRHD and GRMHD codes (see, e.g., Hawley et al. 1984; Porth et al. 2017; Weih et al. 2020).

The effects of shear viscosity – such as the one arising from turbulent motion – have first been considered by Turolla & Nobili (1989), who however adopted a description in terms of the general-relativistic NS equations. However, already in this simplified setup, Turolla & Nobili (1989) have

pointed out the numerous subtleties and highly nontrivial behaviour of the problem of stationary viscous accretion onto a black hole. Hence, to the best of our knowledge, the problem of stationary, spherically symmetric accretion of bulk viscous fluids onto nonrotating black holes using second-order dissipative-hydrodynamics framework has not been considered before. We here use the solution of this problem obtained from the corresponding system of ordinary differential equations (ODEs) to test our implementation of bulk viscosity in BHAC in a curved spacetime geometry. Details on the derivation and solution of the ODEs can be found in Appendix B.

We assume the fluid to be a mixture of ionised non-relativistic hydrogen coupled to photons by employing the following EOS (see, e.g., Rezzolla & Zanotti 2013)

$$p = p_M(1 + \alpha). \quad (125)$$

Here,  $p_M$  denotes the pressure of the matter component, which is assumed to be an ideal gas, while the contribution from the radiation component is fixed using the parameter  $\alpha$ . By rearranging Eq. (125), we find that the EOS of the total mixture takes the same form as the EOS for an ideal gas having an effective adiabatic index  $\gamma_e$ :

$$p = (\gamma_e - 1)(e - \rho), \quad (126)$$

where  $\gamma_e = 1 + 2(1 + \alpha)/[3(1 + 2\alpha)]$ . Note that  $e$  is the total energy density of the mixture while  $\rho$  denotes the rest-mass density of the hydrogen ions. The effective adiabatic index  $\gamma_e$  should not be confused with the generalized adiabatic exponent  $\Gamma_1$  which instead is defined through a thermodynamic relation:  $\Gamma_1 := (\partial \ln p / \partial \ln \rho)_{\tilde{s}} = (5/2 + 20\alpha + 16\alpha^2) / [(3/2 + 12\alpha)(1 + \alpha)]$ , where  $\tilde{s}$  denotes the specific entropy (see, e.g., Mihalas & Mihalas 1984; Rezzolla & Zanotti 2013). In addition, the effective adiabatic index  $\gamma_e$  can be expressed through the well-known generalized adiabatic exponent  $\Gamma_3$  which is defined by  $\Gamma_3 - 1 := (\partial \ln T / \partial \ln \rho)_{\tilde{s}} = (1 + 4\alpha) / (3/2 + 12\alpha)$ :

$$\gamma_e = 1 + \frac{9 - 7\Gamma_3}{11 - 9\Gamma_3}. \quad (127)$$

The temperature can be obtained from the ideal-fluid law for the matter component  $p_M = 2(k_B/m_p)\rho T$  which yields:

$$T = \frac{1}{2(1 + \alpha)} \frac{m_p}{k_B} \frac{p}{\rho}, \quad (128)$$

where  $m_p$  denotes the proton mass. Note the appearance of a factor 2 in the denominator coming from the electrons in our charge-neutral plasma. Furthermore, we use a modification of the formula for radiative bulk viscosity given by Weinberg (1971) and Sawyer (2006)

$$\zeta = 4\zeta_0\sigma_{\text{SB}}T^4\tau_{\text{mfp}}\left(\frac{4}{3} - \gamma_e\right)^2, \quad (129)$$

where  $\sigma_{\text{SB}}$  is the Stefan-Boltzmann constant and  $\tau_{\text{mfp}} := m_p\rho^{-1}\sigma_{\text{T}}^{-1}$  the mean free time for a

Model	$\zeta_0$	$\tau_0 [10^{-12}]$
<i>low</i> $\zeta$	160	1.0
<i>medium</i> $\zeta$	16,000	1.0
<i>high</i> $\zeta$	104,000	1.0
<i>low</i> $\tau_{\Pi}$	16,000	0.06
<i>high</i> $\tau_{\Pi}$	16,000	50

**Table 1.** Summary of the various models evolved and their corresponding parameters  $\zeta_0$  and  $\tau_0$ .

photon in the mixture. The constant  $\sigma_T$  denotes the Thomson scattering cross-section. The dimensionless constant  $\zeta_0$  is essentially arbitrary and used here to explore the regimes of low and high bulk viscosities. For the relaxation time  $\tau_{\Pi}$  we choose the parametrization:

$$\tau_{\Pi} = \tau_0 \frac{M}{|\dot{M}|} \left( \frac{r}{2M} \right)^3, \quad (130)$$

where  $r$  denotes the circumference radius in Schwarzschild coordinates,  $M$  the mass of the black hole,  $\dot{M}$  the accretion rate, and  $\tau_0$  is a dimensionless parameter to study short and long relaxation times. Note that in Eq. (130) the relaxation time increases cubically with radius. Adopting this choice has turned out to be necessary to prevent the rapid growth of non-equilibrium effects near the sonic point, which can yield unphysical solutions.

All of the models considered have the sonic point  $r_s$  at  $200 M$ , a black-hole mass of  $M = 3M_{\odot}$ , and  $\alpha = 1$ , which then yields  $\gamma_e = 1.44$ . Furthermore, we set the constants of motion  $\dot{M}$  and  $\mathcal{B}$  from their inviscid values computed at  $r_s = 200 M$ , i.e.,  $\dot{M} = -0.01582$  and  $\mathcal{B} = -1.00192$  in code units. Note that we use a polytropic EOS to solve the inviscid case where the polytropic constant of the fluid mixture is given by  $k = 2(1 + \alpha)T_{\infty}\rho_{\infty}^{1-\gamma_e}$  with asymptotic values  $\rho_{\infty} = 2 \times 10^{-9} \text{ g cm}^{-3}$  and  $T_{\infty} = 1.5 \times 10^5 \text{ K}$ . We recall that  $\mathcal{B}$  is the viscous analogue of the relativistic Bernoulli constant  $-hu_t$ ; (see Appendix B for a definition). Our code units are defined by setting  $m_p/k_B = 1$  and  $k = 1$ . In these units, a polytropic EOS with polytropic index  $\gamma_e$  passing through the pair  $(\rho_{\infty}, T_{\infty})$  is simply given by  $p = \rho^{\gamma_e}$ , where  $T$  and  $p$  are related through Eq. (128). In this way, the calculation of the corresponding inviscid accretion problem simplifies because without dissipative losses the accretion process of an ideal gas is isentropic and can be described by a polytropic EOS.

In the following, we consider five different accretion cases, whose parameters are given in Table 1. We employ a grid of 10,000 cells, which ranges from  $1.5M$  to  $1,000 M$  using horizon-penetrating Kerr-Schild coordinates and show profiles at a time  $10,000 M$  unless stated otherwise.

The inviscid solution for the temperature  $T$ , together with the *high*  $\zeta$  and *low*  $\tau$  models are

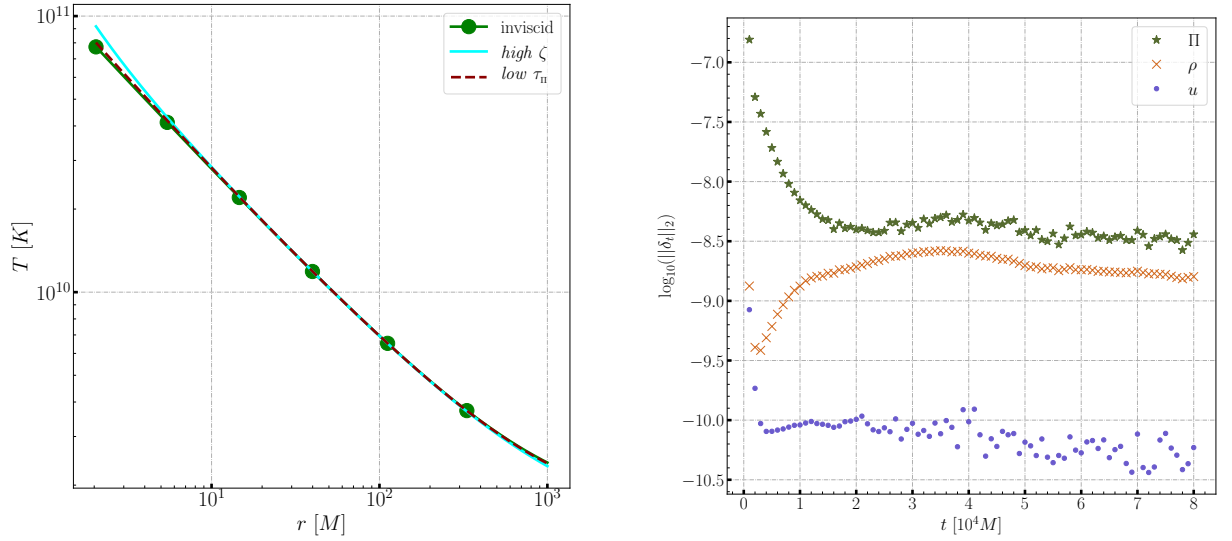


**Figure 3.** *Left:* Temperature  $T$  as a function of the circumference radius  $r$  in units of  $M$  and at time  $10,000 M$ . Shown are the inviscid solution (filled circles) and the models with *high*  $\zeta$  (solid line) and *low*  $\tau$  (dashed line), respectively. Note that deviations from the inviscid solution increase towards the event horizon and that the sonic point is at  $r_s = 200 M$ . *Right:*  $L_2$ -norm of the relative time variation  $\delta_t$  for the bulk-viscosity pressure  $\Pi$  (stars), the rest-mass density  $\rho$  (crosses), and the primitive fluid velocity  $u$  (filled circles) shown as a function of time for the *medium*  $\zeta$  model set using 20,000 grid cells.

shown in the left panel of Fig. 3. To verify that our calculation reaches a stationary state, we show in the right panel of Fig. 3 the logarithm of the  $L_2$ -norm of the relative time variation  $\delta_t$  for the rest-mass density  $\rho$ , the primitive fluid velocity  $u$  and the bulk-viscosity pressure  $\Pi$  as a function of time for the *medium*  $\zeta$  model using 20,000 grid cells. For each quantity  $\phi$ , the relative time variation is defined as  $\delta_t \phi(t) := 1 - \phi(t - 10 M) / \phi(t)$ . In essence, the right panel of 3 shows that, although the fluid was not stationary in the beginning of the evolution, it reaches an approximately stationary state for late times. The small but nonzero value of the relative differences at late times is due to low-amplitude, small-scale oscillations generated at the outer boundary of the numerical domain. We note that after performing a self-convergence test we were able to recover the correct global convergence order of BHAC, i.e.,  $\approx 2$  (see Porth et al. 2017). Local self-convergence tests show that the convergence order is very close to two for small radii, while it exhibits small oscillations around two for large radii, with amplitude that increases towards the outer boundary.

The left panel of Fig. 4 displays the radial profiles of the temperature for the various viscous models when compared to the values obtained from the inviscid solution. As can be seen from the solid lines – which refer to the *low*, *medium* and *high*  $\zeta$  models – the viscous fluid is hotter near the horizon and colder at larger radii than the corresponding inviscid fluid. In particular, for the *high*  $\zeta$  model the temperature at the horizon can be up to  $\sim 18\%$  larger than in the inviscid model. A similar behaviour can be seen also for the dashed lines, which refer to the *low* and *high*  $\tau_\Pi$  models. Shown instead in the right panel of Fig. 4 is the corresponding comparison in the

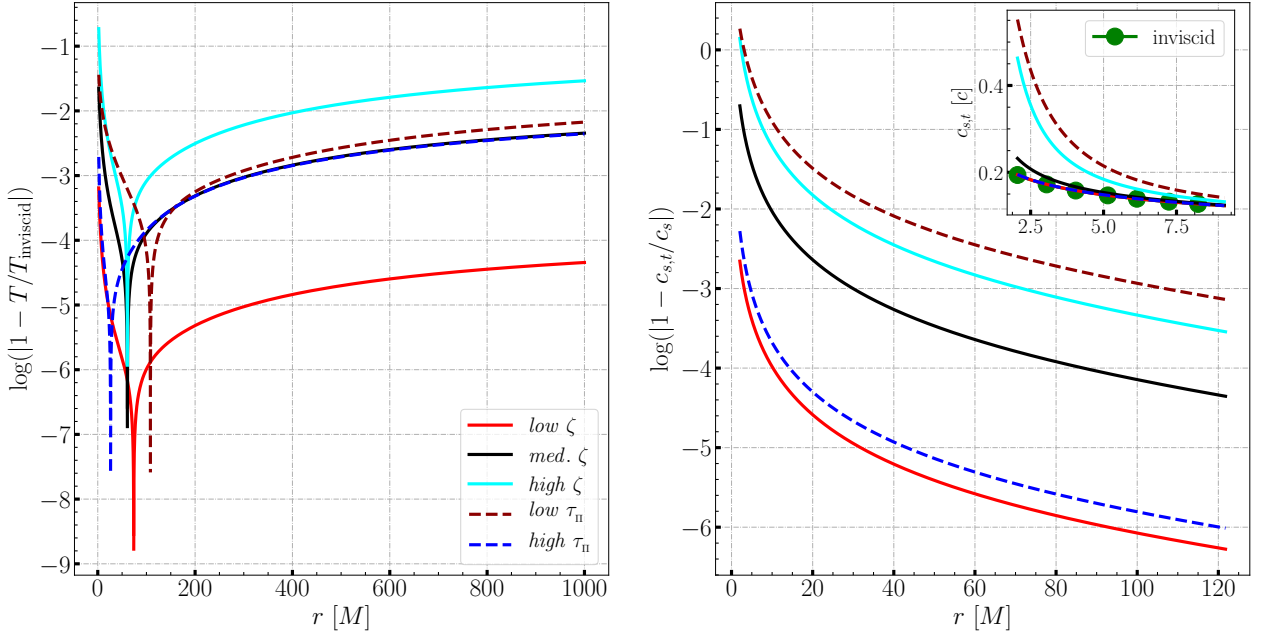


**Figure 4.** *Left:* Relative difference between the temperature  $T$  of the viscous models and the corresponding inviscid model. Note that the differences clearly increase with the increase of the bulk viscosity and that the relative difference changes sign somewhere outside the event horizon. *Right:* Same as on the left but for the sound speed. Reported in the inset is the actual value of the total sound speed near the event horizon, which shows considerable deviations from the inviscid solution.

case of viscous speed of sound when analysed very close to the event horizon. The excess can be up to a factor of almost three for the *low*  $\tau_{\Pi}$  model and a factor of  $\sim 2.3$  for the *high*  $\zeta$  model, reaching viscous sound speeds above 0.5 and 0.4, respectively (see inset). In general, and as can be intuitively expected, solutions with high bulk viscosities and low relaxation times tend to have larger temperatures and viscous sound speeds, and hence larger deviations from the inviscid case.

Figure 5 shows radial profiles of the relativistic “inverse Reynolds number”  $\Pi/\rho h$  (left panel, solid and dashed lines) and of the bulk-viscosity pressure normalized to the corresponding NS value  $\Pi/\Pi_{\text{NS}}$  (right panel, solid and dashed lines). Note that for all models  $\Pi/\rho h$  assumes small but finite values at large radii, decreases when moving inwards and then increases again sharply close to the horizon. The overall magnitude of  $\Pi/\rho h$  is very sensitive to the parameter  $\zeta_0$  (cf. *low*, *medium*, and *high*  $\zeta$  models), while  $\tau_0$  seems to play a marginal role. On the other hand,  $\tau_0$  controls the location of the sharp increase (cf. cases *medium*  $\zeta$ , *low*  $\tau_{\Pi}$ , and *high*  $\tau_{\Pi}$ ). Note that most models approach their corresponding NS values near the horizon, while the rate at which this happens is again controlled by  $\tau_0$ . This can be seen in the right panel of Fig. 5, where models with different  $\tau_0$  show different behaviour. In particular, for the models *low*  $\zeta$ , *medium*  $\zeta$ , and *high*  $\zeta$ , the bulk-viscosity pressure reaches nearly  $\sim 80\%$  of the NS value, while the corresponding value for the *high*  $\tau_{\Pi}$  model is considerably smaller and of the order of  $\sim 10\%$ . Note also that the *low*  $\tau_{\Pi}$  model reaches a maximum of  $\sim 92\%$ , but not exactly at the horizon; this is most likely a behaviour due

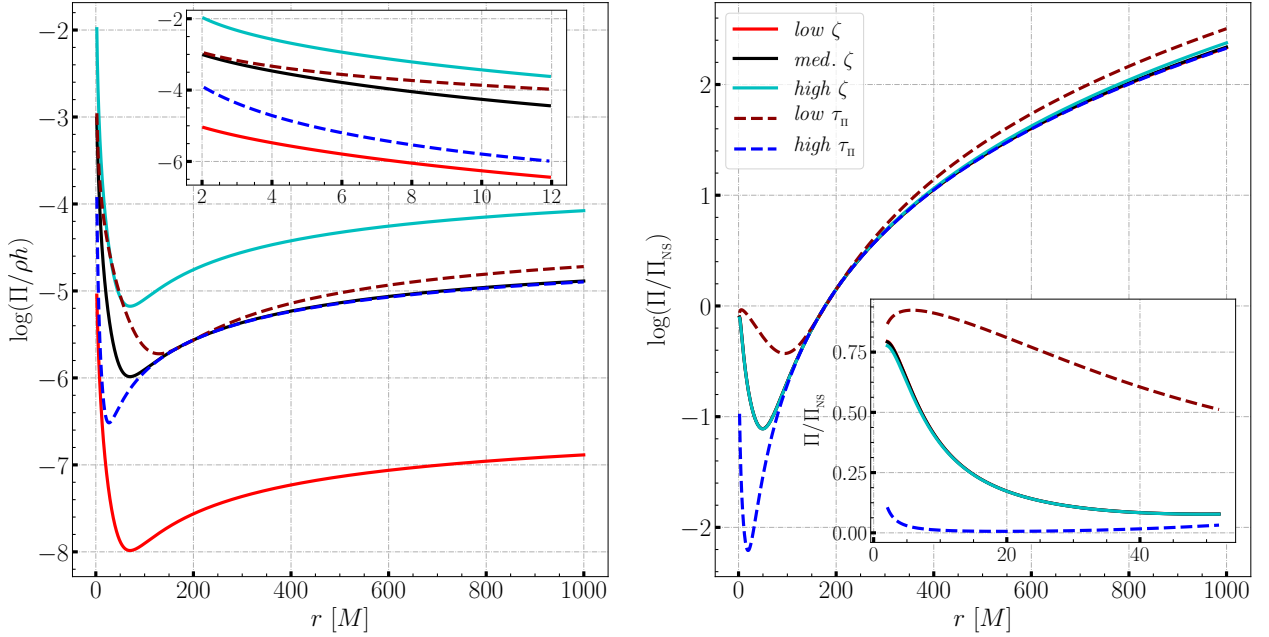


**Figure 5.** *Left:* radial profiles of the ratio of the bulk-viscosity pressure over the enthalpy density (i.e., inverse Reynolds number). Solid lines of different colours refer to models with *low*  $\zeta$ , *medium*  $\zeta$ , and *high*  $\zeta$ ; dashed lines of different colours refer to models with *low*  $\tau_\Pi$  and *high*  $\tau_\Pi$ , respectively. The inset reports the same quantities but near the event horizon. *Right:* radial profiles of the ratio of the bulk-viscosity pressure over the corresponding NS value. Solid and dashed lines follow the same convention as in the left panel, and inset reports the same quantities but near the event horizon.

to a cancellation error near the horizon for the solution obtained by BHAC, since it is absent in the initial solution.

As a concluding remark we note that there are analogies between the late-time behaviour realised in longitudinally expanding fluids, such as the Bjorken flow, and the near-horizon properties of the accretion solution considered here. In both cases, in fact, the solution tends to the corresponding NS value (for late times in the case of the Bjorken flow and for  $r \sim 2M$  in the case of accretion). This behaviour suggests that while the parameter  $\zeta_0$  controls the magnitude of first-order non-equilibrium effects – which in the case of the accretion develop mostly in strong-gravity regions –  $\tau_0$  controls the degree to which  $\Pi$  approaches its NS value. Of course, these considerations are based on the examination of the simplest form of a bulk viscosity. A more extensive investigation of possible initial conditions, transport coefficients and additional source terms in the bulk-viscosity pressure equation will yield a deeper insight into the accretion process of viscous matter that, as pointed out by [Turolla & Nobili \(1989\)](#), is far from being trivial.

## 8 SUMMARY AND CONCLUSION

After having reviewed the various approaches developed over the years to model relativistic dissipative fluids, we have derived a general-relativistic 3+1 flux-conservative formulation of the

second-order dissipative-hydrodynamics equations first suggested by Israel (1976) and Hiscock & Lindblom (1983) (i.e., the **HL83** set of GRDHD equations). The new set of equations derived in this way provides a comprehensive and complete way of including causal dissipative effects in general-relativistic calculations.

Although a 3+1 formulation of a reduced version of the **HL83** set of GRDHD equations was already proposed by Peitz & Appl (1997) and Peitz & Appl (1999)<sup>7</sup>, the work presented here extends the results of Peitz and Appl in three important ways. First, our set of equations is complete and does not neglect terms that are considered to play a less significant role (see Appendix A for a comparison of the system presented here with other formulations). Second, the equations presented are cast into a flux-conservative form suitable for numerical implementation. Finally, also the coupling terms between the different dissipative currents are rewritten a 3+1 form. As a result, the full system given in Hiscock & Lindblom (1983) can now be readily implemented in modern numerical-relativity codes and evolved numerically.

As a way to test the new set of equations, we have proceeded with the implementation in the GRMHD code BHAC of a reduced version of the equations describing fluids with zero shear and heat currents, and used them against a number of tests in flat and curved background metrics.

In the first case, we have first considered the one-dimensional, longitudinally boost-invariant motion of a viscous fluid, such as the one produced in an ultrarelativistic collision of two ions. This expansion, first proposed by Bjorken for an inviscid fluid, is a standard testbed and can be solved analytically. Overall, we find that the numerical solutions agree well with the analytical solutions, with a relative difference that is  $\sim 10^{-7}$  for all the values of viscosity considered. As an additional flat-spacetime test, we have explored the solution of a shock-tube problem for an ultra-relativistic gas of gluons for different values of the ratio  $\zeta/s$ , with  $\zeta$  and  $s$  being bulk-viscosity coefficient and the entropy density, respectively. Also in this case, when comparing the solutions with those obtained with methods based on the direct solution of the relativistic Boltzmann equation, we find a very good agreement up to a ratio of  $\zeta/s \lesssim 0.133$ , which is already in a regime where a dissipative-hydrodynamics framework breaks down.

Finally, as a general-relativistic test we have considered for the first time the problem of stationary, spherically symmetric accretion of bulk viscous fluids onto nonrotating black holes within a second-order dissipative-hydrodynamics framework. Starting from initial conditions obtained

<sup>7</sup> In Peitz & Appl (1997) and Peitz & Appl (1999), all terms including products of dissipative currents, i.e.,  $\Pi$ ,  $q$  and  $\pi$ , and first-order gradients of the primary fluid variables are set to zero in Eqs. (8) – (10).



from the solution of a non-trivial set of ODEs (see Appendix B for details), we evolve the fluid with different values of the bulk-viscosity coefficient and of the relaxation time. Given the non-triviality of this testbed, we recommend it as a standard benchmark for those codes wishing to include dissipative effects in the general-relativistic modelling of compact objects. Overall, we find that the solution obtained by BHAC can deviate from the corresponding inviscid solution with differences  $\lesssim 19\%$  for the temperature and  $\sim 200\%$  for the sound speed. In addition, the bulk-viscosity pressure is highly sensitive to the bulk-viscosity coefficient, exhibiting deviations of up to three orders of magnitude near the event horizon depending on whether the viscosity is large or small. We also show that, although BHAC is able to maintain a quasi-stationarity in the solution and shows global second-order convergence, it does not converge to the reference solution with increasing grid resolution because of the influence of a finite-size computational domain. Interestingly, we note analogies between the late-time behaviour in the Bjorken and accretion flows. In both cases, in fact, the solution tends to the corresponding NS value, with this happening at late times in the Bjorken flow, and near the horizon in the case of accretion onto a black hole.

As a concluding remark we note that although the 3+1 formulation presented here, and its corresponding discretisation, offers a viable path to the inclusion of non-equilibrium effects in general-relativistic simulations of compact objects, short relaxation times as well as the required temporal and spatial discretization of the source terms in the full system may lead to stiff equations, whose solution will not be feasible with simple explicit schemes. We leave the examination of more sophisticated numerical techniques for future work, where mixed explicit-implicit (IMEX) time integrators (see, e.g., Palenzuela et al. 2009; Dionysopoulou et al. 2013; Weih et al. 2020) will be considered.

## ACKNOWLEDGEMENTS

We thank Masoud Shokri, Elias Most, Hector Olivares and Lukas Weih for useful discussions. Support comes in part from HGS-HIRe for FAIR; the LOEWE-Program in HIC for FAIR; “PHAROS”, COST Action CA16214; the ERC Synergy Grant “BlackHoleCam: Imaging the Event Horizon of Black Holes” (Grant No. 610058); the Deutsche Forschungsgemeinschaft (DFG, German Research Foundation) through the CRC-TR 211 “Strong-interaction matter under extreme conditions” - project number 315477589 - TRR 211.

**References**

- Abbott B. P., et al., 2017a, *Phys. Rev. Lett.*, **119**, 161101
- Abbott B. P., et al., 2017b, *Astrophys. J. Lett.*, **848**, L13
- Abbott B. P., et al., 2018, *Physical Review Letters*, **121**, 161101
- Afshordi N., Paczyński B., 2003, *Astrophys. J.*, **592**, 354
- Aguilera-Miret R., Viganò D., Carrasco F., Miñano B., Palenzuela C., 2020, *Phys. Rev. D*, **102**, 103006
- Alcubierre M., 2008, *Introduction to 3 + 1 Numerical Relativity*. Oxford University Press, Oxford, UK, doi:10.1093/acprof:oso/9780199205677.001.0001
- Alford M. G., Haber A., 2020, arXiv e-prints, p. arXiv:2009.05181
- Alford M. G., Bovard L., Hanauske M., Rezzolla L., Schwenzer K., 2018, *Phys. Rev. Lett.*, **120**, 041101
- Alford M., Harutyunyan A., Sedrakian A., 2020, *Particles*, p. arXiv:2006.07975
- Andersson N., Comer G. L., 2015, *Classical and Quantum Gravity*, **32**, 075008
- Andersson N., Comer G. L. C., 2020, arXiv e-prints, p. arXiv:2008.12069
- Annala E., Gorda T., Kurkela A., Vuorinen A., 2018, *Phys. Rev. Lett.*, **120**, 172703
- Baier R., Romatschke P., Son D. T., Starinets A. O., Stephanov M. A., 2008, *Journal of High Energy Physics*, **2008**, 100
- Baiotti L., Rezzolla L., 2017, *Rept. Prog. Phys.*, **80**, 096901
- Baiotti L., Giacomazzo B., Rezzolla L., 2008, *Phys. Rev. D*, **78**, 084033
- Bauswein A., Just O., Janka H.-T., Stergioulas N., 2017, *Astrophys. J. Lett.*, **850**, L34
- Bemfica F. S., Disconzi M. M., Noronha J., 2019a, *Phys. Rev. D*, **100**, 104020
- Bemfica F. S., Disconzi M. M., Noronha J., 2019b, *Phys. Rev. Lett.*, **122**, 221602
- Bemfica F. S., Disconzi M. M., Hoang V., Noronha J., Radosz M., 2020, arXiv e-prints, p. arXiv:2005.11632
- Bernhard J. E., Moreland J. S., Bass S. A., 2019, *Nature Physics*, **15**, 1113
- Betz B., Henkel D., Rischke D. H., 2009, *Progress in Particle and Nuclear Physics*, **62**, 556
- Betz B., Denicol G., Koide T., Molnar E., Niemi H., Rischke D., 2011, *EPJ Web Conf.*, **13**, 07005
- Biswas R., Dash A., Haque N., Pu S., Roy V., 2020, *Journal of High Energy Physics*, **2020**, 171
- Bjorken J. D., 1983, *Phys. Rev. D*, **27**, 140
- Bondi H., 1952, *Mon. Not. R. Astron. Soc.*, **112**, 195
- Bouras I., Molnar E., Niemi H., Xu Z., El A., Fochler O., Greiner C., Rischke D. H., 2009a, *Phys. Rev. Lett.*, **103**, 032301
- Bouras I., Molnár E., Niemi H., Xu Z., El A., Fochler O., Greiner C., Rischke D. H., 2009b, *Nuclear Phys. A*, **830**, 741
- Bouras I., Molnar E., Niemi H., Xu Z., El A., Fochler O., Greiner C., Rischke D. H., 2010, *Phys. Rev.*, **C82**, 024910
- Brito C. V., Denicol G. S., 2020, *Phys. Rev. D*, **102**, 116009
- Burns E., 2020, *Living Reviews in Relativity*, **23**, 4
- Busza W., Rajagopal K., van der Schee W., 2018, *Annual Review of Nuclear and Particle Science*, **68**, 339
- Carter B., 1989, in Anile A., Choquet-Bruhat Y., eds, *Lecture Notes in Mathematics*, Vol. 1385, *Relativistic Fluid Dynamics*. Springer Berlin / Heidelberg, pp 1–64, <http://dx.doi.org/10.1007/BFb0084028>
- Cowperthwaite P. S., et al., 2017, *Astrophys. J. Lett.*, **848**, L17
- De S., Finstad D., Lattimer J. M., Brown D. A., Berger E., Biwer C. M., 2018, *Physical Review Letters*, **121**, 091102
- Del Zanna L., et al., 2013, *European Physical Journal C*, **73**, 2524
- Denicol G. S., Kodama T., Koide T., Mota P., 2008a, *Journal of Physics G: Nuclear and Particle Physics*, **35**, 115102
- Denicol G. S., Kodama T., Koide T., Mota P., 2008b, *Phys. Rev. C*, **78**, 034901
- Denicol G. S., Molnár E., Niemi H., Rischke D. H., 2012a, *The European Physical Journal A*, **48**, 170
- Denicol G. S., Niemi H., Molnár E., Rischke D. H., 2012b, *Phys. Rev. D*, **85**, 114047
- Denicol G., Niemi H., Bouras I., Molnar E., Xu Z., Rischke D., Greiner C., 2014, *Phys. Rev. D*, **89**, 074005
- Dionysopoulou K., Alic D., Palenzuela C., Rezzolla L., Giacomazzo B., 2013, *Phys. Rev. D*, **88**, 044020
- Disconzi M. M., Kephart T. W., Scherrer R. J., 2017, *International Journal of Modern Physics D*, **26**, 1750146

- Drout M. R., et al., 2017, *Science*, **358**, 1570
- Duez M. D., Liu Y. T., Shapiro S. L., Stephens B. C., 2004, *Phys. Rev. D*, **69**, 104030
- Duez M. D., et al., 2020, *Phys. Rev. D*, **102**, 104050
- Eckart C., 1940, *Phys. Rev.*, **58**, 919
- Event Horizon Telescope Collaboration et al., 2019, *Astrophys. J. Lett.*, **875**, L1
- Fambri F., Dumbser M., Köppel S., Rezzolla L., Zanotti O., 2018, *Mon. Not. R. Astron. Soc.*, **477**, 4543
- Fujibayashi S., Kiuchi K., Nishimura N., Sekiguchi Y., Shibata M., 2018, *The Astrophysical Journal*, **860**, 64
- Gabbana A., Plumari S., Galesi G., Greco V., Simeoni D., Succi S., Tripiccion R., 2020, *Phys. Rev. C*, **101**, 064904
- Gourgoulhon E., 2012, 3+1 Formalism in General Relativity. Lecture Notes in Physics, Berlin Springer Verlag Vol. 846, Springer, doi:10.1007/978-3-642-24525-1
- Hairer E., Wanner G., 1996, Solving Ordinary Differential Equations II - Stiff and Differential-Algebraic Problems, 2nd edn. Springer
- Hawley J. F., Smarr L. L., Wilson J. R., 1984, *Astrophys. J.*, **277**, 296
- Hebert F., Kidder L. E., Teukolsky S. A., 2018, *Phys. Rev. D*, **98**, 044041
- Hiscock W. A., Lindblom L., 1983, *Annals of Physics*, **151**, 466
- Hiscock W. A., Lindblom L., 1985, *Phys. Rev. D*, **31**, 725
- Hiscock W. A., Lindblom L., 1987, *Phys. Rev. D*, **35**, 3723
- Hoult R. E., Kovtun P., 2020, *Journal of High Energy Physics*, **2020**, 67
- Inghirami G., Del Zanna L., Beraudo A., Moghaddam M. H., Becattini F., Bleicher M., 2016, *European Physical Journal C*, **76**, 659
- Inghirami G., Del Zanna L., Beraudo A., Haddadi Moghaddam M., Becattini F., Bleicher M., 2018, in *Journal of Physics Conference Series*. p. 012043, doi:10.1088/1742-6596/1024/1/012043
- Israel W., 1976, *Annals of Physics*, **100**, 310
- Israel W., Stewart J. M., 1979, *Annals of Physics*, **118**, 341
- Jaiswal A., 2013, *Phys. Rev. C*, **87**, 051901
- Jaiswal A., Bhalerao R. S., Pal S., 2013, *Phys. Rev. C*, **87**, 021901
- Jordan D. W., Smith P., 2007, *Nonlinear Ordinary Differential Equations : An Introduction for Scientists and Engineers*. Oxford University Press, Oxford, UK
- Kiuchi K., Kyutoku K., Sekiguchi Y., Shibata M., 2018, *Phys. Rev. D*, **97**, 124039
- Koeppel S., Bovard L., Rezzolla L., 2019, *Astrophys. J. Lett.*, **872**, L16
- Kovtun P., 2019, *Journal of High Energy Physics*, **2019**, 34
- Landau L. D., Lifshitz E. M., 2004, *Fluid Mechanics, Course of Theoretical Physics, Volume 6*. Elsevier Butterworth-Heinemann, Oxford
- Malik T., Alam N., Fortin M., Providência C., Agrawal B. K., Jha T. K., Kumar B., Patra S. K., 2018, *Physical Review C*, **98**, 035804
- Mandal I., Ray A. K., Das T. K., 2007, *Mon. Not. R. Astron. Soc.*, **378**, 1400
- Margalit B., Metzger B. D., 2017, *Astrophys. J. Lett.*, **850**, L19
- McNelis M., Bazow D., Heinz U., 2021, arXiv e-prints, p. arXiv:2101.02827
- Michel F. C., 1972, *Ap&SS*, **15**, 153
- Mihalas D., Mihalas B., 1984, *Foundations of radiation hydrodynamics*
- Mizuno Y., et al., 2018, *Nature Astronomy*,
- Montaña G., Tolós L., Hanauske M., Rezzolla L., 2019, *Phys. Rev. D*, **99**, 103009
- Most E. R., Weih L. R., Rezzolla L., Schaffner-Bielich J., 2018, *Phys. Rev. Lett.*, **120**, 261103
- Most E. R., Papenfort L. J., Rezzolla L., 2019, *Mon. Not. R. Astron. Soc.*, **490**, 3588
- Muronga A., 2004, *Phys. Rev. C*, **69**, 034903
- Nobili L., Turolla R., Zampieri L., 1991, *Astrophys. J.*, **383**, 250
- Olivares H., et al., 2020, *MNRAS*, **497**, 521
- Palenzuela C., Lehner L., Reula O., Rezzolla L., 2009, *Mon. Not. R. Astron. Soc.*, **394**, 1727
- Paschalidis V., 2017, *Classical and Quantum Gravity*, **34**, 084002
- MNRAS **000**, 1–55 (2021)

- Peitz J., Appl S., 1997, *Mon. Not. R. Astron. Soc.*, **286**, 681
- Peitz J., Appl S., 1999, *Class. Quantum Grav.*, **16**, 979
- Porth O., Olivares H., Mizuno Y., Younsi Z., Rezzolla L., Moscibrodzka M., Falcke H., Kramer M., 2017, *Computational Astrophysics and Cosmology*, **4**, 1
- Pu S., Koide T., Rischke D. H., 2010, *Phys. Rev. D*, **81**, 114039
- Pu S., Roy V., Rezzolla L., Rischke D. H., 2016, *Phys. Rev. D*, **93**, 074022
- Radice D., 2017, *Astrophys. J. Lett.*, **838**, L2
- Radice D., 2020, *Symmetry*, **12**, 1249
- Radice D., Rezzolla L., 2012, *Astron. Astrophys.*, **547**, A26
- Radice D., Perego A., Bernuzzi S., Zhang B., 2018a, *Mon. Not. R. Astron. Soc.*, **481**, 3670
- Radice D., Perego A., Zappa F., Bernuzzi S., 2018b, *Astrophys. J. Lett.*, **852**, L29
- Radice D., Perego A., Hotokezaka K., Fromm S. A., Bernuzzi S., Roberts L. F., 2018c, *Astrophys. J.*, **869**, 130
- Raithel C., Özel F., Psaltis D., 2018, *Astrophys. J.*, **857**, L23
- Ray A. K., Bhattacharjee J. K., 2002, *Phys. Rev. E*, **66**, 066303
- Rezzolla L., Zanotti O., 2013, *Relativistic Hydrodynamics*. Oxford University Press, Oxford, UK, doi:10.1093/acprof:oso/9780198528906.001.0001
- Rezzolla L., Most E. R., Weih L. R., 2018, *Astrophys. J. Lett.*, **852**, L25
- Romatschke P., Romatschke U., 2019, *Relativistic Fluid Dynamics In and Out of Equilibrium: And Applications to Relativistic Nuclear Collisions*. Cambridge Monographs on Mathematical Physics, Cambridge University Press, doi:10.1017/9781108651998
- Roy V., Pu S., Rezzolla L., Rischke D., 2015, *Physics Letters B*, **750**, 45
- Ruiz M., Shapiro S. L., Tsokaros A., 2018, *Phys. Rev. D*, **97**, 021501
- Rusanov V. V., 1961, *J. Comput. Math. Phys. USSR*, **1**, 267
- Sawyer R. F., 2006, *Phys. Rev. D*, **74**, 043527
- Shibata M., Hotokezaka K., 2019, *Annual Review of Nuclear and Particle Science*, **69**, 41
- Shibata M., Kiuchi K., Sekiguchi Y.-i., 2017, *Phys. Rev. D*, **95**, 083005
- Shibata M., Zhou E., Kiuchi K., Fujibayashi S., 2019, *Phys. Rev. D*, **100**, 023015
- Siegel D. M., Ciolfi R., Harte A. I., Rezzolla L., 2013, *Phys. Rev. D R*, **87**, 121302
- Taghinavaz F., 2020, *JHEP*, **08**, 119
- Tews I., Margueron J., Reddy S., 2018, *Physical Review C*, **98**, 045804
- Turolla R., Nobili L., 1989, *Astrophys. J.*, **342**, 982
- Van P., Biro T., 2012, *Phys. Lett. B*, **709**, 106
- Viganò D., Aguilera-Miret R., Carrasco F., Miñano B., Palenzuela C., 2020, *Phys. Rev. D*, **101**, 123019
- Weih L. R., Olivares H., Rezzolla L., 2020, *Mon. Not. R. Astron. Soc.*, **495**, 2285
- Weinberg S., 1971, *Astrophys. J.*, **168**, 175
- Wolfram Research I., 2020, *Mathematica*, Version 12.1, <https://www.wolfram.com/mathematica>

## APPENDIX A: REVIEW OF SECOND-ORDER RELATIVISTIC DISSIPATIVE HYDRODYNAMICS

This Appendix serves the scope of providing a guidance in comparing our reference second-order formulation of general-relativistic dissipative hydrodynamics originally suggested by [Hiscock & Lindblom \(1983\)](#) with other formulations that have appeared in the literature, i.e., the formulations

by Israel & Stewart (1979) (hereafter **IS79**), by Denicol et al. (2012a) (hereafter **DMNR12**)<sup>8</sup>, and by Baier et al. (2008) (hereafter **rBRSSS08**). Since these formulations often adopt different notations that makes it hard to compare them, we introduce a generalized notation for the various transport coefficients, whose terminology is given in Table A1. Furthermore, since the equations of **HL83** are chosen as our reference equations, we use upper-case letters for transport coefficients appearing in **HL83**; the only exception to this rule will be made for the relaxation times. Furthermore, since the comparison needs to distinguish terms of first and second order, we introduce the following dimensionless numbers: the Knudsen number

$$\text{Kn} := \frac{l_{\text{micro}}}{L_{\text{macro}}}, \quad (\text{A1})$$

where  $l_{\text{micro}}$  and  $L_{\text{macro}}$  are the microscopic lengthscale given by the mean-free-path of the microscopic constituents of the fluid and the macroscopic lengthscale given by the distance over which gradients of primary fluid variables appear, respectively. Furthermore, the inverse Reynolds numbers are given by

$$\text{R}_{\Pi}^{-1} := \frac{|\Pi|}{p+e}, \quad \text{R}_n^{-1} := \frac{|n^\mu|}{n}, \quad \text{R}_\pi^{-1} := \frac{|\pi^{\mu\nu}|}{p+e}. \quad (\text{A2})$$

Note that in the Eckart frame the inverse Reynolds number  $\text{R}_n^{-1}$  is replaced by

$$\text{R}_q^{-1} := \frac{|q^\mu|}{p+e} \sim \mathcal{O}(\text{R}_n^{-1}). \quad (\text{A3})$$

Using these dimensionless numbers, we can identify the order of the terms given in Table A2 according to the following classification:

$$\mathcal{O}(\text{R}_i^{-1}, \text{Kn}) := \mathcal{O}_1, \quad \mathcal{O}(\text{R}_i^{-1} \text{Kn}) := \mathcal{O}_{\text{RK}}, \quad \mathcal{O}(\text{R}_i^{-1} \text{R}_j^{-1}) := \mathcal{O}_{2\text{R}}, \quad \mathcal{O}(\text{Kn}^2) := \mathcal{O}_{2\text{K}}. \quad (\text{A4})$$

In this way, following the convention of Denicol et al. (2012b), we refer to terms of order  $\mathcal{O}_1$  as being of first order, while all other terms are referred to as being of second order.

With these definitions made, we next proceed to the actual comparison which will take place by first briefly reviewing each of the formulations considered (Sec. A1–A4) and then proceeds with the actual comparison (Sec. A5).

<sup>8</sup> Note that there is another frequently used second-order GRDHD formulation proposed by Denicol et al. (2012b) and often referred to as the “DNMR” formulation. We will not use this formulation for our comparison here since the formulation by Denicol et al. (2012b) is in the Landau frame and we instead consider the formulations adopting the Eckart frame for our comparison.

transport coefficients	description
$\tau_\Pi, \tau_q, \tau_\pi$	relaxation times for bulk viscosity, heat conduction and shear viscosity, respectively
$\delta_j^i$ or $\Delta_j^i$	transport coefficients for gradients of the fluid velocity $\mathbf{u}$
$l_j^i$ or $L_j^i$	transport coefficients for gradients of the dissipative currents
$\lambda_j^i$ or $\Lambda_j^i$	transport coefficients for the contribution of gradients of $\rho$ and $p$
$\varphi_j^i$	transport coefficients for the contribution of contracted dissipative currents
$g_j^i$	transport coefficients in front of geometrical quantities, i.e. $R_{\mu\nu\lambda\rho}$ , $R_{\mu\nu}$ or $R$

**Table A1.** Generalized notation for the transport coefficients. Shown on the left are the newly introduced symbols, while a description of which fluid field it appears in combination with is shown on the right. The upper index indicates which dissipative current the transport coefficient belongs to, e.g.,  $\delta_2^\Pi$  is the second transport coefficient expressing the coupling to a gradient of the fluid velocity in the constitutive equation for the bulk-viscosity pressure. Upper-case letters indicate that the corresponding transport coefficient occurs in the **HL83** formulation, while lower case letters indicate that it is set to zero in **HL83**.

## A1 Israel and Stewart 1979 (IS79)

The equations for the dissipative currents of **IS79** read as follows

$$\tau_\Pi \dot{\Pi} = \Pi_{\text{LNS}} - \Pi + \delta_1^\Pi q^\mu a_\mu + L_1^\Pi \nabla_\mu q^\mu, \quad (\text{A5})$$

$$\tau_q \dot{q}^{\langle\mu\rangle} = q_{\text{NS}}^{\mu} - q^\mu + \delta_1^q \Pi a^\mu + \delta_2^q \pi^{\mu\nu} a_\nu + \delta_3^q \omega^{\mu\nu} q_\nu + L_1^q \nabla^{\langle\mu\rangle} \Pi + L_2^q \nabla_\nu \pi^{\langle\mu\rangle\nu}, \quad (\text{A6})$$

$$\tau_\pi \dot{\pi}^{\langle\mu\nu\rangle} = \pi_{\text{LNS}}^{\mu\nu} - \pi^{\mu\nu} + \delta_1^\pi q^{\langle\mu} a^{\nu\rangle} + \delta_2^\pi \pi^{\lambda\langle\mu} \omega^{\nu\rangle}{}_\lambda + L_1^\pi \nabla^{\langle\mu} q^{\nu\rangle}. \quad (\text{A7})$$

Here,  $\Pi_{\text{LNS}}$  and  $\pi_{\text{LNS}}^{\mu\nu}$  denote the NS values of the dissipative currents evaluated in the Landau frame. Equations (A5), (A6) and (A7) correspond to equations (7.1a), (7.1b) and (7.1c) of [Israel & Stewart \(1979\)](#), respectively. This set of equations was derived using the Boltzmann equation for the single-particle distribution function  $f$ , parametrized in the form

$$y(x^\mu, p^i) := \ln \left[ \frac{f(x^\mu, p^i)}{A_1} \right], \quad (\text{A8})$$

$$y(x^\mu, p^i) := \frac{\mu}{T} + \epsilon + \left( \frac{u_\lambda}{T} + \frac{\epsilon_\lambda}{m} \right) p^\lambda + \frac{1}{m^2} \epsilon_{\lambda\rho} p^\lambda p^\rho, \quad (\text{A9})$$

$$A_1 := 1 + A_2 f(x^\mu, p^i), \quad A_2 \in \{-1, 0, +1\}, \quad (\text{A10})$$

where  $p^0 = p^0(p^i, m)$  is the on-shell energy of the particles,  $A_2 = -1(+1)$  refers to fermions (bosons) so that  $A_2 \rightarrow 0$  corresponds to the limit yielding the Boltzmann distribution, and  $m$  is the mass of the particles.

The functions  $\epsilon$ ,  $\epsilon_\lambda$  and  $\epsilon_{\lambda\rho}$  are off-equilibrium corrections. Note that we recover the standard Fermi, Bose and Boltzmann local-equilibrium distributions for  $\epsilon, \epsilon_\lambda, \epsilon_{\lambda\rho} = 0$ . The single-particle distribution  $f$  contains 14 independent variables ( $T, \mu$ , the three independent components of  $u^\mu$  and the nine independent components of the functions  $\epsilon, \epsilon_\lambda$  and  $\epsilon_{\lambda\rho}$ ). These are one-to-one matched to the components of  $J^\mu$  and  $T^{\mu\nu}$ . The system of conservation equations, corresponding to the equations of motion for the first and second moment of  $f$ , is closed by employing the equation of motion for the third moment of  $f$ , leading to relaxation-type equations for the dissipative currents.

The fact that 14 independent variables occur in the equations of motion is also referred to as the “14-moment approximation”.

We should recall that in the derivation of **IS79** two approximations are made. First, they neglected second-order terms proportional to  $\nabla^\mu \rho$  and  $\Theta$ . Following the derivation from the second law of thermodynamics, these terms arise from gradients of the transport coefficients and are generally of the form (see, e.g., the equation for the shear-stress tensor)  $\propto \pi^{\mu\nu} u_\lambda \bar{I}^\lambda$  and  $\propto q^{\langle\mu} \bar{I}^{\nu\rangle}$ , where  $\bar{I}^\mu$  is a linear combination of gradients of transport coefficients that can be related to gradients of the chosen pair of thermodynamical variables  $\{T, \mu\}$  or  $\{\rho, p\}$ . In general, these terms can be further decomposed by using the first-order version of the conservation laws (1) and (2):

$$\dot{\rho} \propto \Theta, \quad (\text{A11})$$

$$a^\mu \propto \nabla^{\langle\mu} p, \quad (\text{A12})$$

$$\dot{e} \propto \Theta, \quad (\text{A13})$$

where, again,  $\dot{\mathbf{A}} := (\mathbf{u} \cdot \nabla) \mathbf{A} = u^\mu \nabla_\mu \mathbf{A}$ . By choosing the pair  $\{\rho, p\}$  as our thermodynamical variables and exploiting Eqs. (A11) – (A13), the following relations are valid to second-order

$$\pi^{\mu\nu} u_\lambda \bar{I}^\lambda \propto \pi^{\mu\nu} \Theta, \quad (\text{A14})$$

$$q^{\langle\mu} \bar{I}^{\nu\rangle} \propto b_1 q^{\langle\mu} a^{\nu\rangle} + b_2 q^{\langle\mu} \nabla^{\nu\rangle} \rho, \quad (\text{A15})$$

where  $b_1$  and  $b_2$  denote scalar functions of the pair  $\{\rho, p\}$ . Hence, the missing terms in **IS79** proportional to  $\nabla^\mu \rho$  and  $\Theta$  are of the form  $\propto \pi^{\mu\nu} \Theta$  and  $\propto q^{\langle\mu} \nabla^{\nu\rangle} \rho$ , while the term  $b_1 q^{\langle\mu} a^{\nu\rangle}$  could be absorbed in the transport coefficient  $\delta_1^\pi$ .

Second, there are terms of the form  $\propto \pi^{\lambda\langle\mu} \sigma^{\nu\rangle}{}_\lambda$  and  $\propto \Pi \sigma^{\mu\nu}$ , appearing for instance in the equation for the shear-stress tensor that are also apparently missing in the **IS79** formulation. The existence of these terms was first pointed out by [Betz et al. \(2011\)](#), which were subsequently included in the **DMNR12** formulation (see below).

## A2 Hiscock and Lindblom 1983 (HL83)

When using a generalized notation, the evolution equations (8)–(10) for the dissipative currents in the **HL83** formulation can be written as

$$\tau_\Pi \dot{\Pi} = \Pi_{\text{NS}} - \Pi + \Delta_1^\Pi \Pi \Theta + L_1^\Pi \nabla_\mu q^\mu + \Lambda_1^\Pi \Pi u_\mu I_1^\mu + \Lambda_2^\Pi q_\mu I_2^\mu, \quad (\text{A16})$$

$$\begin{aligned} \tau_q \dot{q}^{\langle\mu} \rangle &= q_{\text{NS}}^\mu - q^\mu + \Delta_1^q q^\mu \Theta + L_1^q \nabla^{\langle\mu} \Pi + L_2^q \nabla_\nu \pi^{\langle\mu} \pi^{\nu\rangle} + \Lambda_1^q q^\mu u_\nu I_3^\nu \\ &\quad + \Lambda_2^q \Pi I_2^{\langle\mu} \rangle + \Lambda_3^q \pi^\mu{}_\nu I_4^{\nu\rangle}, \end{aligned} \quad (\text{A17})$$

$$\tau_\pi \dot{\pi}^{\langle\mu\nu\rangle} = \pi_{\text{NS}}^{\mu\nu} - \pi^{\mu\nu} + \Delta_1^\pi \pi^{\mu\nu} \Theta + L_1^\pi \nabla^{\langle\mu} q^{\nu\rangle} + \Lambda_1^\pi \pi^{\mu\nu} u_\lambda I_5^\lambda + \Lambda_2^\pi q^{\langle\mu} I_4^{\nu\rangle}. \quad (\text{A18})$$

where the currents  $I_i^\mu$  are given by

$$I_1^\mu := \nabla^\mu (\tau_\Pi / \zeta T) , \quad (\text{A19})$$

$$I_2^\mu := \nabla^\mu (\alpha_0 / T) , \quad (\text{A20})$$

$$I_3^\mu := \nabla^\mu (\tau_q / \kappa T^2) , \quad (\text{A21})$$

$$I_4^\mu := \nabla^\mu (\alpha_1 / T) , \quad (\text{A22})$$

$$I_5^\mu := \nabla^\mu (\tau_\pi / \eta T) . \quad (\text{A23})$$

In similarity with Sec. A1, we can use the first-order relations (A11)–(A13) to further decompose the terms in (A16)–(A18) that include the currents  $I_i^\mu$  and obtain

$$\Pi u_\mu I_1^\mu \propto \Pi \Theta , \quad (\text{A24})$$

$$q_\mu I_2^\mu \propto b_3 q_\mu a^\mu + b_4 q_\mu \nabla^\mu \rho , \quad (\text{A25})$$

$$q^\mu u_\nu I_3^\nu \propto q^\mu \Theta , \quad (\text{A26})$$

$$\Pi I_2^{\langle \mu \rangle} \propto b_4 \Pi a^\mu + b_5 \Pi \nabla^{\langle \mu \rangle} \rho , \quad (\text{A27})$$

$$\pi^\mu{}_\nu I_4^\nu \propto b_6 \pi^\mu{}_\nu a^\nu + b_7 \pi^\mu{}_\nu \nabla^\nu \rho , \quad (\text{A28})$$

$$\pi^{\mu\nu} u_\lambda I_5^\lambda \propto \pi^{\mu\nu} \Theta , \quad (\text{A29})$$

$$q^{\langle \mu} I_4^{\nu \rangle} \propto b_8 q^{\langle \mu} a^{\nu \rangle} + b_9 q^{\langle \mu} \nabla^{\nu \rangle} \rho , \quad (\text{A30})$$

where, again, the quantities  $b_3$ – $b_9$  are scalar functions of  $\rho$  and  $p$ .

### A3 Denicol et al. 2012a (DMNR12)

The equations for the dissipative currents of the **DMNR12** formulation are

$$\tau_\Pi \dot{\Pi} = \Pi_{\text{NS}} - \Pi + \Delta_1^\Pi \Pi \Theta + \delta_1^\Pi q^\mu a_\mu + \delta_2^\Pi \pi^{\mu\nu} \sigma_{\mu\nu} + L_1^\Pi \partial_\mu q^\mu + \Lambda_2^\Pi q_\mu I_6^\mu , \quad (\text{A31})$$

$$\begin{aligned} \tau_q \dot{q}^{\langle \mu \rangle} &= q_{\text{NS}}^\mu - q^\mu + \Delta_1^q q^\mu \Theta + \delta_1^q \Pi a^\mu + \delta_2^q \pi^{\mu\nu} a_\nu + \delta_3^q \omega^{\mu\nu} q_\nu + \delta_4^q \sigma^{\mu\nu} q_\nu \\ &\quad + L_1^q \partial^{\langle \mu \rangle} \Pi + L_2^q \partial_\nu \pi^{\langle \mu \rangle \nu} + \Lambda_2^q \Pi I_6^{\langle \mu \rangle} + \Lambda_3^q \pi^\mu{}_\nu I_6^\nu , \end{aligned} \quad (\text{A32})$$

$$\begin{aligned} \tau_\pi \dot{\pi}^{\langle \mu \nu \rangle} &= \pi_{\text{NS}}^{\mu\nu} - \pi^{\mu\nu} + \Delta_1^\pi \pi^{\mu\nu} \Theta + \delta_1^\pi q^{\langle \mu} a^{\nu \rangle} + \delta_2^\pi \pi^{\lambda \langle \mu} \omega^{\nu \rangle}{}_\lambda + \delta_3^\pi \pi^{\lambda \langle \mu} \sigma^{\nu \rangle}{}_\lambda \\ &\quad + \delta_4^\pi \Pi \sigma^{\mu\nu} + L_1^\pi \partial^{\langle \mu} q^{\nu \rangle} + \Lambda_2^\pi q^{\langle \mu} I_6^{\nu \rangle} . \end{aligned} \quad (\text{A33})$$

Equations (A31), (A32) and (A33) correspond to equations (128), (138) and (153) of Denicol et al. (2012a), respectively, when the Eckart frame is chosen as the frame of reference, i.e., when



$V^\mu = 0$  and  $W^\mu = q^\mu$ . Notice that the terms including the current  $I_6^\mu$  can be decomposed as

$$q_\mu I_6^\mu \propto b_{10} q_\mu a^\mu + b_{11} q_\mu \nabla^\mu \rho, \quad (\text{A34})$$

$$\Pi I_6^{\langle \mu \rangle} \propto b_{10} \Pi a^\mu + b_{11} \Pi \nabla^{\langle \mu \rangle} \rho, \quad (\text{A35})$$

$$\pi^\mu{}_\nu I_6^\nu \propto b_{10} \pi^\mu{}_\nu a^\nu + b_{11} \pi^\mu{}_\nu \nabla^\nu \rho, \quad (\text{A36})$$

$$q^{\langle \mu} I_6^{\nu \rangle} \propto b_{10} q^{\langle \mu} a^{\nu \rangle} + b_{11} q^{\langle \mu} \nabla^{\nu \rangle} \rho, \quad (\text{A37})$$

where  $I_6^\mu := \partial^\mu \left( \frac{\mu}{T} \right)$  and  $b_{10}, b_{11}$  are scalar functions of  $\rho$  and  $p$ .

Note that Eqs. (A31)–(A33) have been derived for a flat spacetime with signature  $(+, -, -, -)$ <sup>9</sup>, so that the comoving derivative is  $\dot{\mathbf{A}} = u^\mu \partial_\mu \mathbf{A}$ . Hence, in the comparison we will carry out in Sec. A5 the covariant derivatives in our general-relativistic formulation have to be replaced with a simple partial derivative when comparing to DMNR12.

We recall that in the derivation of the DMNR12 formulation, the full off-equilibrium distribution function is decomposed as

$$f(x^\mu, p^i) = f_0(x^\mu, p^i) + \delta f(x^\mu, p^i), \quad (\text{A38})$$

where  $f_0$  is the local-equilibrium distribution function and  $\delta f$  denotes the deviation from it. One then defines the so-called generalized irreducible moments of order  $r$  of  $\delta f$  as

$$\rho_r^{\mu_1 \dots \mu_l} := \int \frac{g d^3 p}{(2\pi)^3 p^0} (E)^r p^{\langle \mu_1} \dots p^{\mu_l \rangle} \delta f, \quad (\text{A39})$$

where  $g$  is the number of internal degrees of freedom and  $E$  is defined by  $p^\mu =: E u^\mu + p^{\langle \mu}$ . The full off-equilibrium distribution function can now be expanded in momentum space in a basis of irreducible tensors  $p^{\langle \mu_1} \dots p^{\mu_l \rangle}$  and orthogonal polynomials in  $E$ , where the generalized irreducible moments appear as coefficients. Some of these moments are directly connected to the dissipative currents, e.g.,

$$\Pi = -\frac{m^2}{3} \rho_0 = -\frac{m^2}{3} \int \frac{g d^3 p}{(2\pi)^3 p^0} \delta f, \quad (\text{A40})$$

$$q^\mu = \rho_1^\mu = \int \frac{g d^3 p}{(2\pi)^3 p^0} E p^\mu \delta f, \quad (\text{A41})$$

$$\pi^{\mu\nu} = \rho_0^{\mu\nu} = \int \frac{g d^3 p}{(2\pi)^3 p^0} p^{\langle \mu} p^{\nu \rangle} \delta f. \quad (\text{A42})$$

Inserting Eq. (A38) into the special-relativistic version of the Boltzmann equation leads to an equation of motion for  $\delta f$ ,

$$\delta \dot{f} = -\dot{f}_0 - \frac{1}{E} p^{\langle \mu} \partial_\mu (f_0 + \delta f). \quad (\text{A43})$$

This equation is then used to evaluate the comoving derivatives of the generalized irreducible

<sup>9</sup> This choice introduces a sign difference in some quantities, e.g.,  $\pi_{\text{NS}}^{\mu\nu}$ , which are instead computed with the signature  $(-, +, +, +)$ .

moments (A39) and leads to an infinite set of evolution equations for the latter. When this infinite system is truncated at the lowest order – corresponding to the 14-moment approximation – it leads to the **IS79**-like equations, which have been given above by Eqs. (A31)–(A33).

However, this procedure is ambiguous because, once the 14-moment approximation is applied, it is possible to obtain a closed evolution equation of the desired dissipative current from any choice of  $r$  in Eq. (A39), for the irreducible moment of tensor rank corresponding to that of the respective dissipative current<sup>10</sup>. This can be seen from the  $r$ -dependence of the transport coefficients in Tables A3 and A4, which reflects the choice of the moment equation. The transport coefficients of **IS79** are obtained if one sets  $r = 3$  for the scalar moment,  $r = 2$  for the vector moment and  $r = 1$  for the tensor moment. Microphysical properties of the system are encoded in the transport coefficients obtained from a moment expansion of the collision integral of the Boltzmann equation. Instead of applying the 14-moment approximation, a power-counting scheme in Knudsen and inverse Reynolds numbers is used by Denicol et al. (2012b) to truncate the system.

#### A4 Baier et al. 2008 (rBRSSS08)

The equations for the dissipative currents of the **rBRSSS08** formulation read as follows [here we use the version presented by Romatschke & Romatschke (2019), where they appear as Eq. (2.122)]<sup>11</sup>

$$\begin{aligned} \tau_{\Pi} \dot{\Pi} = & \Pi_{\text{NS}} - \Pi + \delta_3^{\Pi} \omega^{\mu\nu} \omega_{\mu\nu} + \lambda_1^{\Pi} I_{7\langle\mu} I_7^{\mu\rangle} + \varphi_1^{\Pi} \pi^{\mu\nu} \pi_{\mu\nu} + \varphi_2^{\Pi} \Pi^2 \\ & + g_1^{\Pi} R + g_2^{\Pi} u^{\mu} u^{\nu} R_{\mu\nu}, \end{aligned} \quad (\text{A44})$$

$$\begin{aligned} \tau_{\pi} \dot{\pi}^{\langle\mu\nu\rangle} = & \pi_{\text{NS}}^{\mu\nu} - \pi^{\mu\nu} + \Delta_1^{\pi} \pi^{\mu\nu} \Theta + \delta_2^{\pi} \pi^{\lambda\langle\mu} \omega^{\nu\rangle}_{\lambda} + \delta_5^{\pi} \omega^{\langle\mu}_{\lambda} \omega^{\nu\rangle\lambda} + \lambda_1^{\pi} I_7^{\langle\mu} I_7^{\nu\rangle} \\ & + \varphi_1^{\pi} \pi^{\lambda\langle\mu} \pi^{\nu\rangle}_{\lambda} + g_1^{\pi} R^{\langle\mu\nu\rangle} + g_2^{\pi} u_{\lambda} u_{\rho} R^{\lambda\langle\mu\nu\rangle\rho}. \end{aligned} \quad (\text{A45})$$

Note that we have defined  $I_7^{\mu} := \nabla^{\mu} \ln e$  and that the heat current is absent because these expressions refer to the Landau frame as the reference frame, where the heat currents are zero by definition.

As for the previous formulations, we can use the first-order relations (A11)–(A13) to further

<sup>10</sup> Stated differently, it is possible to derive a relationship between the dissipative currents  $\Pi$ ,  $q^{\mu}$ , and  $\pi^{\mu\nu}$ , which are essentially the irreducible moments  $\rho_0$ ,  $\rho_1^{\mu}$ , and  $\rho_0^{\mu\nu}$ , and all the other  $\rho_r$ ,  $\rho_r^{\mu}$ , and  $\rho_r^{\mu\nu}$ , for any index  $r$ . As a result, there is ambiguity because it is possible to derive an equation of motion for  $\Pi$ , etc. from the equation of motion for  $\rho_r$ , etc. for any  $r$  and not only for  $r = 0$ .

<sup>11</sup> In Baier et al. (2008) the equations for the dissipative currents have been derived for the case of conformal fluids. Here we present their complete extension to the case of non-conformal fluids.

decompose the terms in Eqs. (A44), (A45) that include the current  $I_7^\mu$  as

$$\begin{aligned} I_{7\langle\mu} I_7^{\mu\rangle} &= I_{7\mu} I_7^\mu + u_\mu I_7^\mu u_\nu I_7^\nu \\ &\propto (b_{12} a_\mu + b_{13} \nabla_\mu \rho) (b_{12} a^\mu + b_{13} \nabla^\mu \rho) + b_{14} \Theta^2 \\ &\propto (b_{12})^2 a_\mu a^\mu + 2b_{12} b_{13} a^\mu \nabla_\mu \rho + (b_{13})^2 \nabla_\mu \rho \nabla^\mu \rho + b_{14} \Theta^2, \end{aligned} \quad (\text{A46})$$

$$I_7^{\langle\mu} I_7^{\nu\rangle} \propto (b_{12})^2 a^{\langle\mu} a^{\nu\rangle} + 2b_{12} b_{13} a^{\langle\mu} \nabla^{\nu\rangle} \rho + (b_{13})^2 \nabla^{\langle\mu} \rho \nabla^{\nu\rangle} \rho, \quad (\text{A47})$$

where, again, the quantities  $b_{12}, b_{13}$  and  $b_{14}$  are scalar functions of  $\rho$  and  $p$ .

The **rBRSSS08** formulation is based on a systematic expansion in terms of gradients of the fluid variables in equilibrium and of the metric  $g_{\mu\nu}$ , hence inheriting purely geometric terms involving the Ricci tensor  $R_{\mu\nu}$  and the Ricci scalar  $R := R^\mu{}_\mu$ . The dissipative currents are then written as a power series in such gradients up to a given order. The individual terms for the shear-stress tensor respect its properties, namely that it is symmetric, trace-free and orthogonal to  $u$ .

A resummation procedure is then applied to obtain relaxation-type equations, e.g., for the shear-stress tensor the first-order relation  $\pi^{\mu\nu} = -2\eta\sigma^{\mu\nu}$  is used to derive

$$u^\lambda \nabla_\lambda \pi^{\langle\mu\nu\rangle} \propto -2\eta u^\lambda \nabla_\lambda \sigma^{\langle\mu\nu\rangle} - b_{15} \sigma^{\mu\nu} \Theta, \quad (\text{A48})$$

which then leads to hyperbolic equations of motion if the term  $u^\lambda \nabla_\lambda \sigma^{\langle\mu\nu\rangle}$  is substituted using (A48) in the corresponding parabolic equations of motion. Note that  $b_{15}$  is a scalar function of  $\rho$  and  $p$ , and can be absorbed in the definitions of the transport coefficients. In addition, Eq. (A48) is accurate to second order in the gradients. In this way, the previously acausal behaviour is cured and causality is recovered.

## A5 Comparing different GRDHD formulations

After having introduced and reviewed four different second-order formulations of the equations of GRDHD, namely, **IS79**, **HL83**, **DMNR12** and **rBRSSS08**, we next proceed with a comparison of the sets of evolution equations for the dissipative currents. In order to facilitate the identification of the transport coefficients in our notation with the transport coefficients in the original notations, we have distinguished between the different currents  $I_i^\mu$ , as well as the kinematic acceleration  $a^\mu$  so far. However, as one can see from the first-order relations (A11)–(A13), a further reduction is possible by using equations (A24)–(A30), (A34)–(A37) and (A46), (A47), respectively. To this scope, we choose the pair  $\{\rho, p\}$  as our thermodynamical variables and write every gradient as a linear combination of the pair  $\{a^\mu, \partial^{\langle\mu} \rho\}$ . We apply this reduction in order to compare **IS79**, **DMNR12** and **rBRSSS08** with **HL83** in Table A2. Thus, it is convenient to introduce the new

Formulation	Order	bulk-pressure equation		heat-current equation		shear-tensor equation	
		—	+	—	+	—	+
IS79	$\mathcal{O}_{\text{RK}}$	$\Pi\Theta$		$q^\mu\Theta$	$\omega^{\mu\nu}q_\nu$	$\pi^{\mu\nu}\Theta$	$\pi^{\lambda\langle\mu}\omega^{\nu\rangle}_\lambda$
		$q_\mu\mathcal{I}^\mu$		$\Pi\mathcal{I}^{\langle\mu}$ $\pi^\mu{}_\nu\mathcal{I}^\nu$		$q^{\langle\mu}\mathcal{I}^{\nu\rangle}$	
DMNR12	$\mathcal{O}_{\text{RK}}$		$\pi^{\mu\nu}\sigma_{\mu\nu}$		$\omega^{\mu\nu}q_\nu$ $\sigma^{\mu\nu}q_\nu$		$\pi^{\lambda\langle\mu}\omega^{\nu\rangle}_\lambda$ $\pi^{\lambda\langle\mu}\sigma^{\nu\rangle}_\lambda$ $\Pi\sigma^{\mu\nu}$
		$\Pi\Theta$ $\nabla_\mu q^\mu$ $q_\mu a^\mu$ $q_\mu\mathcal{I}^\mu$		N/A	N/A	$\nabla^{\langle\mu}q^{\nu\rangle}$ $q^{\langle\mu}a^{\nu\rangle}$ $q^{\langle\mu}\mathcal{I}^{\nu\rangle}$	$\pi^{\lambda\langle\mu}\omega^{\nu\rangle}_\lambda$
rBRSS08	$\mathcal{O}_{2\text{K}}$		$\Theta^2$ $\omega^{\mu\nu}\omega_{\mu\nu}$ $a_\mu a^\mu$ $a_\mu\mathcal{I}^\mu$ $\mathcal{I}_\mu\mathcal{I}^\mu$				$\omega^{\lambda\langle\mu}\omega^{\nu\rangle}_\lambda$ $a^{\langle\mu}a^{\nu\rangle}$ $a^{\langle\mu}\mathcal{I}^{\nu\rangle}$ $\mathcal{I}^{\langle\mu}\mathcal{I}^{\nu\rangle}$
			$\pi^{\mu\nu}\pi_{\mu\nu}$				$\pi^{\lambda\langle\mu}\pi^{\nu\rangle}_\lambda$
			$\Pi^2$				
			$R$				$R^{\langle\mu\nu\rangle}$
		N/A	$u^\mu u^\nu R_{\mu\nu}$				$u_\lambda u_\rho R^{\lambda\langle\mu\nu\rangle\rho}$

**Table A2.** Comparison between different formalisms. Terms that are included in the **HL83** formulation but are missing in the given formulation are coloured in red and listed under ‘—’. Similarly, those terms that are absent in the **HL83** formulation but are included in the other approaches are coloured in blue and listed under ‘+’. Terms that differ only by a scalar function of  $\rho$  and  $p$  are not counted as missing, as potential differences can be absorbed in the definition of the transport coefficients. For each formulation we also use different rows to reflect the classification within the scheme with respect to the order of Knudsen or inverse Reynolds number (A4). Finally, terms without any symbol are not classified because they do not occur in the corresponding approach.

definition

$$\mathcal{I}^\mu := \nabla^\mu \rho. \quad (\text{A49})$$

Notice that this reduction procedure leads to differences in some transport coefficients, which are captured by the previously introduced scalar functions  $\{b_i\}_{i \in [1,14]}$ .

Table A2 presents a quick overview of the various formulations considered, whose denomination appears in the first column. The table is written such that terms that are included in the **HL83** formulation but are missing in the set we want to compare with are coloured in red and listed under ‘—’. Similarly, those terms that are absent in the **HL83** formulation but are included in the other approaches are coloured in blue and listed under ‘+’. Furthermore, terms that differ only by a scalar function of  $\rho$  and  $p$  are not counted as missing, as potential differences can be absorbed in the definition of the transport coefficients. Furthermore, to facilitate the classification of the various terms within the scheme (A4), i.e., with respect to the order of Knudsen or inverse

Reynolds number  $\mathcal{O}_1$ ,  $\mathcal{O}_{\text{RK}}$ ,  $\mathcal{O}_{2\text{R}}$ , and  $\mathcal{O}_{2\text{K}}$ , they are collected on different rows. Finally, terms without any symbol are not classified because they do not occur in the corresponding approach.

Note that the **rBRSSS08** formulation includes second-order terms, but does not distinguish between  $\eta\sigma^{\mu\nu}\Pi$  and  $\zeta\pi^{\mu\nu}\Theta$ . However, these are not the only second-order terms present in the **rBRSSS08** formulation. Another difference is of course the presence of terms associated with the curvature of spacetime, which are absent in **DMNR12**. Clearly, these terms cannot be classified by a certain order within the scheme (A4). However, if  $g_{\mu\nu}$  is considered as an equilibrium fluid variable, then these terms can be seen as of second order in Knudsen number. Finally, we recall that the **rBRSSS08** formulation is derived in the Landau frame, where the heat currents are zero.

As a corollary to this comparison, we report in Tables A3 and A4 a list of all the transport coefficients in our and in the original notation, while the definition of all  $I_i^\mu$  is given in Table A5.

## APPENDIX B: DETAILS ON VISCOUS BLACK-HOLE ACCRETION

Given the very limited use and knowledge of the stationary solution of the spherically symmetric equations of GRDHD in a Schwarzschild spacetime, we here review the basic mathematical expressions and the strategy employed to obtain a numerical solution in the presence of a critical point.

### B1 Equations of GRDHD

We recall that the equations of GRDHD are given by Eqs. (1), (2) where  $J^\mu = J_{\text{PF}}^\mu$ , and  $T^{\mu\nu}$  is given by Eq. (4), together with Eq. (99) in the case in which the heat current and the shear-stress tensor are set to zero. By demanding the equations to be stationary and spherically symmetric, i.e., all state variables are functions of the circumference radius  $r$  only and the fluid four-velocity has the form  $u^\mu = (u^t, u, 0, 0)^T$ , it is possible to obtain the following coupled, nonlinear system

IS79	HL83	DMNR12	rBRSSS08	local	source
$-1/3 \zeta_V u_{E \mu}^\mu$	$-\zeta\Theta$	$-\zeta^r\Theta$	$-\zeta\nabla_\mu^\perp u^\mu$	$\Pi_{\text{NS}}$	-
$\frac{\kappa T}{\eta\beta} \Delta_\lambda^\mu \alpha_{ \mu}$	$-\kappa T(\nabla^{(\mu} \ln T + \frac{\kappa_q^r \tau_W^r}{\psi_r^W \tau_V^r \beta_0^2 h_0^2} \nabla^{(\mu} \alpha_0$		N/A	$q_{\text{NS}}^\mu$	-
$-2\zeta_S \Delta_{(\lambda}^\alpha (u_E) \Delta_{\mu)}^\beta (u_E) u_{\alpha \beta}^E$	$-2\eta\sigma^{\mu\nu}$	$2\eta^r \sigma^{\mu\nu}$	$-\eta\sigma^{\mu\nu}$	$\pi_{\text{NS}}^{\mu\nu}$	-
$1/3 \zeta_V \beta_0$	$\zeta\beta_0$	$\tau_\Pi^r$	$\tau_\Pi$	$\tau_\Pi$	$\dot{\Pi}$
$\kappa T \beta_1$	$\kappa T \beta_1$	$\tau_W^r$	N/A	$\tau_q$	$\dot{q}^{(\mu)}$
$2\zeta_S \beta_2$	$2\eta\beta_2$	$\tau_\pi^r$	$\tau_\pi$	$\tau_\pi$	$\dot{\pi}^{(\mu\nu)}$
0	$-1/2 \tau_\Pi$	$-\tau_\Pi^r \delta_{\Pi\Pi}^r$	0	$\Delta_1^\Pi$	$\Pi\Theta$
$1/3 \zeta_V a'_0$	0	$\tau_\Pi^r \tau_{\Pi W}^r$	0	$\delta_1^\Pi$	$q^\mu a_\mu$
0	0	$\tau_\Pi^r \lambda_{\Pi\pi}^r$	0	$\delta_2^\Pi$	$\pi^{\mu\nu} \sigma_{\mu\nu}$
0	0	0	$\xi_3$	$\delta_3^\Pi$	$\omega^{\mu\nu} \omega_{\mu\nu}$
0	$-1/2 \tau_q$	$-\tau_W^r \delta_{WW}^r$	N/A	$\Delta_1^q$	$q^\mu \Theta$
$\kappa T a_0$	0	$-\tau_W^r \tau_{q\Pi}^r / \psi_r^W$	N/A	$\delta_1^q$	$\Pi a^\mu$
$\kappa T a_1$	0	$-\tau_W^r \tau_{q\pi}^r / \psi_r^W$	N/A	$\delta_2^q$	$\pi^{\mu\nu} a_\nu$
$\kappa T \beta_1 = \tau_q$	0	$\tau_W^r$	N/A	$\delta_3^q$	$\omega^{\mu\nu} q_\nu$
0	0	$-\tau_W^r \lambda_{WW}^r$	N/A	$\delta_4^q$	$\sigma^{\mu\nu} q_\nu$
0	$-1/2 \tau_\pi$	$-2\tau_\pi^r \delta_{\pi\pi}^r$	$-(\tau_\pi d + \bar{\tau}_\pi^*)/(d-1)$	$\Delta_1^\pi$	$\pi^{\mu\nu} \Theta$
$2\zeta_S a'_1$	0	$2\tau_{\pi W}^r \tau_\pi^r$	0	$\delta_1^\pi$	$q^{(\mu} a^{\nu)}$
$4\zeta_S \beta_2 = 2\tau_\pi$	0	$2\tau_\pi^r$	$-\lambda_2/\eta$	$\delta_2^\pi$	$\pi^{\lambda(\mu} \omega^{\nu)}_\lambda$
0	0	$-2\tau_\pi^r \lambda_{\pi\pi}^r$	0	$\delta_3^\pi$	$\pi^{\lambda(\mu} \sigma^{\nu)}_\lambda$
0	0	$2\tau_\pi^r \lambda_{\pi\Pi}^r$	0	$\delta_4^\pi$	$\Pi\sigma^{\mu\nu}$
0	0	$2\tau_\pi^r \lambda_{\pi\Pi}^r$	$\lambda_3$	$\delta_5^\pi$	$\omega^{\lambda(\mu} \omega^{\nu)}_\lambda$
$1/3 \zeta_V \alpha_0$	$\zeta\alpha_0$	$-\tau_\Pi^r l_{\Pi W}^r$	0	$L_1^\Pi$	$\nabla_\mu q^\mu$
$\kappa T \alpha_0$	$\kappa T \alpha_0$	$l_{q\Pi}^r \tau_W^r / \psi_r^W$	N/A	$L_1^q$	$\nabla^{(\mu} \Pi$
$\kappa T \alpha_1$	$\kappa T \alpha_1$	$-l_{q\pi}^r \tau_W^r / \psi_r^W$	N/A	$L_2^q$	$\nabla_\nu \pi^{(\mu} \nu)$
$2\zeta_S a_1$	$2\eta\alpha_1$	$2l_{\pi W}^r \tau_\pi^r$	0	$L_1^\pi$	$\nabla^{(\mu} q^{\nu)}$

**Table A3.** Table of transport coefficients I: we here match the transport coefficients used in this work with the corresponding transport coefficients in the original papers of the **IS79**, **HL83**, **DMNR12**, and **rBRSSS08** formulations.

of ordinary differential equations (ODEs) in Schwarzschild coordinates:

$$\frac{d\rho}{dr} = -\frac{\rho}{r} \frac{M/(\mathcal{E}^2 r) - \Pi r / [(\rho h + \Pi)\tau_\Pi u] - 2u^2/\mathcal{E}^2}{c_{s,t}^2 - u^2/\mathcal{E}^2}, \quad (\text{B1})$$

$$\frac{du}{dr} = \frac{u}{r} \frac{M/(\mathcal{E}^2 r) - \Pi r / [(\rho h + \Pi)\tau_\Pi u] - 2c_{s,t}^2}{c_{s,t}^2 - u^2/\mathcal{E}^2}, \quad (\text{B2})$$

$$\frac{d\Pi}{dr} = -\frac{\Pi (c_{s,t}^2 - u^2/\mathcal{E}^2) / (u\tau_\Pi) + \zeta [M/(\mathcal{E}^2 r) - \Pi r / [(\rho h + \Pi)\tau_\Pi u] - 2u^2/\mathcal{E}^2] / (\tau_\Pi r)}{c_{s,t}^2 - u^2/\mathcal{E}^2}, \quad (\text{B3})$$

$$\frac{dh}{dr} = -\frac{\rho h + \Pi}{\rho r} \frac{[c_{s,t}^2 - (\zeta/\tau_\Pi - \Pi)/(\rho h + \Pi)] [M/(\mathcal{E}^2 r) - \Pi r / [(\rho h + \Pi)\tau_\Pi u] - 2u^2/(\mathcal{E}^2)]}{c_{s,t}^2 - u^2/\mathcal{E}^2}, \quad (\text{B4})$$

IS79	HL83	DMNR12	rBRSSS08	local	source
0	$-1/2 \zeta T$	0	0	$\Lambda_1^\Pi$	$\Pi u_\mu I_i^\mu$
0	$\zeta \gamma_0 T$	$\tau_\Pi^r \lambda_{\Pi W}^r$	0	$\Lambda_2^\Pi$	$q^\mu I_{i\mu}$
0	0	0	$\bar{\xi}_4$	$\lambda_1^\Pi$	$I_{i\mu} I_i^\mu$
0	$-1/2 \kappa T^2$	0	N/A	$\Lambda_1^q$	$q^\mu u^\nu I_{i\nu}$
0	$\kappa T^2 (1 - \gamma_0)$	$\lambda_{q\Pi}^r \tau_W^r / \psi_r^W$	N/A	$\Lambda_2^q$	$\Pi I_i^{(\mu)}$
0	$\kappa T^2 (1 - \gamma_1)$	$\lambda_{q\pi}^r \tau_W^r / \psi_r^W$	N/A	$\Lambda_3^q$	$\pi^{\mu\nu} I_{i\nu}$
0	$-1/2 \eta T$	0	0	$\Lambda_1^\pi$	$\pi^{\mu\nu} u^\lambda I_{i\lambda}$
0	$2\eta \gamma_1 T$	$-2\tau_\pi^r \lambda_{\pi W}^r$	0	$\Lambda_2^\pi$	$q^{(\mu} I_i^{\nu)}$
0	0	0	$\bar{\lambda}_4$	$\lambda_1^\pi$	$I_i^{(\mu} I_i^{\nu)}$
0	0	0	$\xi_1/\eta^2$	$\varphi_1^\Pi$	$\pi^{\mu\nu} \pi_{\mu\nu}$
0	0	0	$\bar{\xi}_2/\zeta^2$	$\varphi_2^\Pi$	$\Pi^2$
0	0	0	$\lambda_1/\eta^2$	$\varphi_1^\pi$	$\pi^{\lambda(\mu} \pi^{\nu)\lambda}$
0	0	0	$\xi_5$	$g_1^\Pi$	$R$
0	0	0	$\xi_6$	$g_2^\Pi$	$u^\mu u^\nu R_{\mu\nu}$
0	0	0	$\kappa$	$g_1^\pi$	$R^{(\mu\nu)}$
0	0	0	$2(\kappa^* - \kappa)$	$g_2^\pi$	$u_\lambda u_\rho R^{\lambda(\mu\nu)\rho}$

**Table A4.** Table of transport coefficients II: the same as Table A3 but for those terms missing in the previous Table. Note that the definitions of the currents  $I_i^\mu$  differ for different formalisms and a summary is given in Table A5.

IS79	HL83	DMNR12	rBRSSS08
N/A	$I_i^\mu = \nabla^\mu (c_i/T), \quad i \in \{1, \dots, 5\}$	$I_6^\mu = \partial^\mu (\frac{\mu}{T})$	$I_7^\mu = \nabla^\mu \ln e$

**Table A5.** Summary of the various definitions of the currents  $I_i^\mu$  given for the four formulations considered here. Note that the **IS79** formulation neglects gradients of transport coefficients and that the coefficients  $c_i$  appearing in the currents of the **HL83** formulation are given by  $c_{\{1, \dots, 5\}} = \{\tau_\Pi/\zeta, \alpha_0, \tau_q/\kappa T, \alpha_1, \tau_\pi/\eta\}$ .

where  $\mathcal{E} := u_t = -\sqrt{1 - 2M/r + u^2}$ . Furthermore, the system is characterised by two conserved quantities, namely, the mass-accretion rate  $\dot{M}$  and the “viscous” Bernoulli constant  $\mathcal{B}$ :

$$\dot{M} := 4\pi \rho u r^2, \quad (B5)$$

$$\mathcal{B} := (\rho h + \Pi) \mathcal{E} / \rho. \quad (B6)$$

Note that in the inviscid limit  $\lim_{\Pi \rightarrow 0} \mathcal{B} = \mathcal{B}_{\text{PF}} := h\mathcal{E} = hu_t$ , where  $\mathcal{B}_{\text{PF}}$  denotes the relativistic, inviscid Bernoulli constant. Using  $\dot{M}$  and  $\mathcal{B}$ , we can express  $\rho$  and  $\Pi$  in terms of  $u$ ,  $h$  and  $r$ :

$$\rho = \dot{M} / (4\pi u r^2), \quad (B7)$$

$$\Pi = \rho \mathcal{B} / \mathcal{E} - \dot{M} h / (4\pi u r^2), \quad (B8)$$

so that the viscous speed of sound becomes

$$c_{s,t}^2 = (\gamma_e - 1) \frac{\mathcal{B} - \mathcal{E}}{\mathcal{B}} + \frac{\zeta}{\tau_\Pi} \frac{4\pi \mathcal{E} u r^2}{\mathcal{B} \dot{M}}, \quad (B9)$$

and Eqs. (B2) and (B4) simplify to

$$\frac{du}{dr} = \frac{u}{r} \frac{M/(\mathcal{E}^2 r) - (\mathcal{B} - \mathcal{E}h)r/(\mathcal{B}\tau_{\text{II}}u) - 2c_{s,t}^2}{c_{s,t}^2 - u^2/\mathcal{E}^2}, \quad (\text{B10})$$

$$\frac{dh}{dr} = -\frac{1}{r} \frac{[(\gamma_e - 1)(\mathcal{B} - \mathcal{E})/\mathcal{E} + (\mathcal{B} - h\mathcal{E})/\mathcal{E}] [M/(\mathcal{E}^2 r) - (\mathcal{B} - \mathcal{E}h)r/(\mathcal{B}\tau_{\text{II}}u) - 2u^2/\mathcal{E}^2]}{c_{s,t}^2 - u^2/\mathcal{E}^2}. \quad (\text{B11})$$

Equations (B10)–(B11) do not have an analytic solution and their non-trivial numerical solution is discussed in more detail in the next section.

## B2 Singular point analysis and integration

The first step in the solution of Eqs. (B10), (B11) is to choose the location of the sonic point  $r_s$ , which is defined as the radial coordinate where  $u^2/\mathcal{E}^2 = c_{s,t}^2$ . This corresponds to the position where the infalling fluid velocity equals that of the speed of sound as observed at rest from spatial infinity, and where Eqs. (B10), (B11) become singular. Because of that, we choose to start the numerical integration procedure directly at  $r_s$  and integrate inward (i.e., supersonic portion) and outward (i.e., subsonic portion) from there. In this way, we can make use of exact results for the states and their first derivatives at the sonic point in order to initialise numerical integration. In the following we will elaborate on the exact method. Using the inviscid solution with a polytropic constant (see discussion in Sec. 7), it is possible to obtain values for  $\dot{M}$  and  $\mathcal{B}_{\text{pf}}$ . In the inviscid case, all state variables at the sonic point are automatically determined by choosing  $r_s$  (see Hawley et al. 1984, for details).

Setting  $\mathcal{B} = \mathcal{B}_{\text{pf}}$  and using the value for  $\dot{M}$  found for the inviscid case, we can compute our initial values at  $r_s$  for the viscous case. As in the inviscid case, we demand that the derivatives at the sonic point constitute a removable singularity. Hence, from equations (B10) and (B11) we find the conditions

$$0 = \frac{M}{\mathcal{E}^2 r} - \frac{\mathcal{B} - \mathcal{E}h}{\mathcal{B}} \frac{r}{\tau_{\text{II}} u} - 2c_{s,t}^2, \quad (\text{B12})$$

$$0 = c_{s,t}^2 - \frac{u^2}{\mathcal{E}^2}. \quad (\text{B13})$$

Numerical root finding via Mathematica (Wolfram Research 2020) yields the values of the radial four-velocity component and of the specific enthalpy at the sonic radius,  $u_s$  and  $h_s$ . Because multiple solutions exist, we select the solution satisfying the conditions:  $u_s < 0$  and  $h_s > 1$ , which was found to be unique for the choice of constant  $\zeta$  and  $\tau_{\text{II}}$ . Next, accurate values for the derivatives  $du/dr$  and  $dh/dr$  are needed at the sonic point because we would otherwise rely on the evaluation of the right-hand side of Eqs. (B10) and (B11) at  $r_s$  for the first step of the integration procedure.



Even though the singularity is removable, numerical errors cause singular behaviour and unreliable values for the derivatives.

Hence, following [Mandal et al. \(2007\)](#) (but see also [Ray & Bhattacharjee 2002](#); [Afshordi & Paczyński 2003](#)) we can treat Eqs. (B10)–(B11) assuming that each function  $u$ ,  $r$ , and  $h$  can be expressed in terms of a parameter  $\xi$ , i.e.,  $u = u(\xi)$ ,  $r = r(\xi)$ ,  $h = h(\xi)$ , such that when writing Eqs. (B10)–(B11) symbolically as  $du/dr = A/B$  and  $dh/dr = C/B$ , they can be effectively rewritten as  $du/d\xi = A$ ,  $dr/d\xi = B$ , and  $dh/d\xi = C$ . More specifically, we express Eqs. (B10)–(B11) symbolically as

$$\frac{dr}{d\xi} = r \left( c_{s,t}^2 - \frac{u^2}{\mathcal{E}^2} \right), \quad (\text{B14})$$

$$\frac{du}{d\xi} = u \left( \frac{M}{\mathcal{E}^2 r} - \frac{\mathcal{B} - \mathcal{E}h}{\mathcal{B}} \frac{r}{\tau_{\text{II}} u} - 2c_{s,t}^2 \right), \quad (\text{B15})$$

$$\frac{dh}{d\xi} = - \left[ (\gamma_e - 1) \frac{\mathcal{B} - \mathcal{E}}{\mathcal{E}} + \frac{\mathcal{B} - h\mathcal{E}}{\mathcal{E}} \right] \left[ \frac{M}{\mathcal{E}^2 r} - \frac{\mathcal{B} - \mathcal{E}h}{\mathcal{B}} \frac{r}{\tau_{\text{II}} u} - 2\frac{u^2}{\mathcal{E}^2} \right]. \quad (\text{B16})$$

Note that  $\xi$  does not have a physical interpretation and should be seen simply as a mathematical parameter. However, with this parameterisation, each of the solutions  $r(\xi)$ ,  $u(\xi)$ , and  $h(\xi)$  can be thought as consisting of two branches on either side of the sonic point: i.e., one branch for  $r < r_s$  and one for  $r > r_s$ . In this way, and as will be found later, the solution at the sonic point can be obtained in the limit  $\xi \rightarrow \pm\infty$ <sup>12</sup>.

Hence, Eqs. (B14)–(B16) effectively represent an independent system whose paths in the  $(u, h, r)$ -space, i.e., the *phase space* of Eqs. (B14)–(B16), correspond to solutions of the original system, i.e., Eqs. (B10) and (B11). Thus, the original system can be viewed as differential equations for the *phase paths* of Eqs. (B14)–(B16). The solution  $(u_s, h_s)$  at the sonic point  $r_s$  constitutes a solution  $(u_s, h_s, r_s)$  of Eqs. (B14)–(B16) at the so-called equilibrium point, where  $du/d\xi = dh/d\xi = dr/d\xi = 0$ . Notice the dependence on the specific choice of  $\zeta = \zeta(u, h, r)$  and  $\tau_{\text{II}} = \tau_{\text{II}}(u, h, r)$ .

Equations (B14)–(B16) can be linearised at the sonic point, i.e.,  $u \approx u_s + \delta u$ ,  $h \approx h_s + \delta h$  and  $r \approx r_s + \delta r$ , to obtain a local solution ([Jordan & Smith 2007](#)). This linearisation procedure and the ansatz  $\delta u = \delta_u \exp(\lambda\xi)$ ,  $\delta h = \delta_h \exp(\lambda\xi)$  and  $\delta r = \delta_r \exp(\lambda\xi)$  leads to an eigenvalue problem, which can be solved numerically ([Wolfram Research 2020](#)). The outcome is a set of three eigenvalues  $\{\lambda_1, \lambda_2, \lambda_3\}$  and eigenvectors with the properties  $\lambda_1 < 0$ ,  $\lambda_2 > 0$  and  $\lambda_3 \approx 0$ . The

<sup>12</sup> This condition follows from the requirement that the perturbation behaves as  $\sim e^{\lambda\xi}$ , where  $\lambda$  is a constant eigenvalue that can be either positive or negative, and that it vanishes at the sonic point; see also below.

corresponding set of local solutions is then

$$\delta u_1(\xi) = (\delta_u)_1 \exp(\lambda_1 \xi); \delta h_1(\xi) = (\delta_h)_1 \exp(\lambda_1 \xi); \delta r_1(\xi) = (\delta_r)_1 \exp(\lambda_1 \xi), \quad (\text{B17})$$

$$\delta u_2(\xi) = (\delta_u)_2 \exp(\lambda_2 \xi); \delta h_2(\xi) = (\delta_h)_2 \exp(\lambda_2 \xi); \delta r_2(\xi) = (\delta_r)_2 \exp(\lambda_2 \xi), \quad (\text{B18})$$

where  $[(\delta_u)_i, (\delta_h)_i, (\delta_r)_i]$  denotes the eigenvector which belongs to the  $i$ -th eigenvalue  $\lambda_i$ . Now, we require the linearised solution to pass through  $(u_s, h_s, r_s)$  exactly, which means that we look for linearised solutions that fulfil  $\delta u_i(\xi) = \delta h_i(\xi) = \delta r_i(\xi) = 0$  for an arbitrary  $\xi$ . Because  $\lambda_3 \approx 0$ , it is not possible to fulfil the requirement  $\delta u_3 = \delta h_3 = \delta r_3 = 0$  for any value of  $\xi$ ; hence, we neglect this eigenvalue. Similarly, because  $\lambda_1$  and  $\lambda_2$  are of opposite signs, superpositions of both sets are not allowed for the same reason. Thus, we recover the desired solution in the limit  $\xi \rightarrow \infty$  for the set (B17) and  $\xi \rightarrow -\infty$  for the set (B18). For each eigenvalue  $i = 1, 2$ , the derivatives are given by  $(du/dr)_s = (\delta_u)_i/(\delta_r)_i$  and  $dh/dr = (\delta_h)_i/(\delta_r)_i$ , respectively, and we select the eigenvalue whose eigenvector yields  $(du/dr)_s > 0$ .

Finally, we start our numerical integration by calculating the first steps on either side of the sonic point, i.e., at  $r_l = r_s - \Delta r$  and  $r_r = r_s + \Delta r$ , employing forward and backward finite-differences of first order with radial stepsize  $\Delta r$ . The integration then proceeds with a fourth-order  $L$ -stable singly diagonally implicit Runge-Kutta (SDIRK) method (see Table 6.5. of [Hairer & Wanner 1996](#) and the corresponding Butcher tableau). It is worth noticing that this method includes an embedded third-order formula and a continuous solution, both of which can be found in [Hairer & Wanner \(1996\)](#). We use a simple fixed-point iteration procedure to solve the implicit equation at each stage, i.e., given the solution at a specific radius  $r_n$ , where  $r_{n+1} = r + \Delta r$  marks the next grid point, we use the solution at  $r_n$  as an initial guess and iterate on the  $k_i$ 's, which are defined by the following general formulas derived assuming the ODE has the form  $dy/dr = f(r, y)$  and an  $s$ -stage Runge-Kutta method

$$y_{n+1} = y_n + \Delta r \sum_{i=1}^s b_i k_i, \quad (\text{B19})$$

$$k_i = f \left( r_n + c_i \Delta r, y_n + h \sum_{j=1}^s a_{ij} k_j \right), \quad i = 1, \dots, s, \quad (\text{B20})$$

and where the coefficients  $\{c_i, a_{ij}, b_i\}$  are given in the form of Butcher tableaux in Table B1. The numerical integration is obtained using 700,000 points on a grid that has a higher resolution in the most delicate portions of the solution, i.e., at the event horizon and at the sonic point. After a cubic-spline interpolation, the numerical solution of the ODEs is then used as initial conditions for the BHAC evolution.

$1/4$	$1/4$				
$3/4$	$1/2$	$1/4$			
$11/20$	$17/50$	$-1/25$	$1/4$		
$1/2$	$371/1360$	$-137/2720$	$15/544$	$1/4$	
$1$	$25/24$	$-49/48$	$125/16$	$-85/12$	$1/4$
<hr/>					
	$25/24$	$-49/48$	$125/16$	$-85/12$	$1/4$

**Table B1.** Butcher tableau for a  $L$ -stable SDIRK method of order 4 [cf., Eqs. (B19)].

This paper has been typeset from a  $\text{\LaTeX}$  file prepared by the author.